IN VITRO CELL WORK OF TWO TYPES OF TARGETED NANOPARTICLES WITH ULTRASOUND TRIGGERING

by

Waad Hussein Abuwatfa

A Thesis presented to the Faculty of the
American University of Sharjah
College of Engineering
In Partial Fulfillment
of the Requirements
for the Degree of

Master of Science in
Chemical Engineering

Sharjah, United Arab Emirates

November 2020

Declaration of Authorship

I declare that this thesis is my own work and, to the best of my knowledge and belief, it does not contain material published or written by a third party, except where permission has been obtained and/or appropriately cited through full and accurate referencing.

Signature: Waad Hussein Abuwatfa

Date: November 1st, 2020

Approval Signatures

We, the undersigned, approve the Master's Thesis of Waad Hussein Abuwatfa

Thesis Title: In Vitro Cell Work of Two Types of Targeted Nanoparticles with Ultrasound Triggering

Date of Defense: 11/11/2020

Name, Title and Affiliation	**Signature**
Dr. Ghaleb Husseini Professor, Department of Chemical Engineering Thesis Advisor	
Dr. Zarook Shareefdeen Professor, Department of Chemical Engineering Thesis Committee Member	
Dr. Nahid Awad Visiting Scholar, PhD Biochemistry Thesis Committee Member	
Dr. Sameer Al-Asheh Head Department of Chemical Engineering	
Dr. Lotfi Romdhane Associate Dean for Graduate Studies and Research College of Engineering	
Dr. Sirin Tekinay Dean College of Engineering	
Dr. Mohamed El-Tarhuni Vice Provost for Graduate Studies Office of Graduate Studies	

Acknowledgements

First and foremost, all praises to Almighty Allah for giving me the strength and ability to complete this work and for all his blessings in every step of my life.

I would like to begin by expressing my earnest gratitude and owe to Dr. Ghaleb Husseini, not only for supervising my thesis, but also for encouraging me and believing in me at times when I did not believe in myself. Thank you for always pushing the bar and providing me with a sense of purpose. I profoundly dedicate this academic success and personal growth to you. This journey would not have been this special without our valuable long talks, your enlightening mentorship, contagious passion, and generous support.

I would also like to acknowledge Dr. Debasmita Mukhopadhyay, Eng. Nour Al Sawaftah and Eng. Vinod Paul great technical guidance, moral support, and insightful contribution to my lab work experience. I am forever blessed for being part of this amazingly synergistic research group. I would also like to thank my close friends for being very supportive through the thin and thick, and always helping me stay focused on my goals.

I would also like to sincerely thank Dr. Amani Al-Othman for being an amazing big sister and a role model for women in engineering. It was a pleasure having the opportunity to teach alongside you. I would also like to thank my committee members, Dr. Nahid Awad and Dr. Zarook Shareefdeen, for their valuable input and comments.

I would also like to thank the Chemical Engineering Department at the American University of Sharjah for supporting my studies with the Graduate Teaching Assistantship (GTA), and the faculty members, who have taught me a great deal about engineering and life as well. My genuine thanks go to Dr. Sameer Al-Asheh for his appreciated guidance and kind words that always inspired me.

Last but not least, my deepest and most heartfelt thanks and love go to my family and parents, to my mom’s silent night prayers and dad’s long waiting hours in the car for me to finish class. Thanks for fostering my passion for learning and always pushing me to excel. I owe everything I have achieved to you; I would have not made it this far without your unconditional love and true endless support.

Dedication

To whom I always want to be the best version of myself for
my sunlight and heartbeat, Mom & Dad…

Abstract

Targeted liposomes have shown promising potential as effective chemotherapeutics delivery vehicles in Smart Drug Delivery Systems (SDDSs). Upon accumulation and internalization at the tumor site, the liposomes need to be potentiated by an external trigger to effectively and controllably release their contents. In this study, synthesis, characterization and *in vitro* cell work of two types of targeted liposomes with ultrasound (US) triggering were considered. The MTT assays of PEGylated liposomes, encapsulating Doxorubicin (DOX), conjugated to human serum albumin (HSA), and Herceptin (HER) were carried out on different cell lines. The size of these nanocarriers was measured using dynamic light scattering (DLS). All three nanoparticles were found to be large unilamellar vesicles (LUVs), with radii of 83.5 ± 0.734 nm, 101 ± 1.56 nm, and 103 ± 1.86 nm for the control, HSA-conjugated, and HER-conjugated liposomes, respectively. The lipid content of the different liposomes was determined using the spectrophotometrical Stewart assay, and the confirmation of the moiety-conjugation was established using the bicinchoninic acid (BCA) assay. The MTT results revealed that functionalizing the liposomes with HSA coupled with US exposure for 20 seconds in a 40-kHz sonicating bath significantly enhanced the nanocarrier's cellular uptake by the MCF-7 (HSA+ breast cancer) cells compared to HeLa (HSA- cervical cancer) cells, with cell viabilities of 15.7 ± 0.613 % and 47.3 ± 0.621% (p-value=8.05×10^{-7}), respectively. As for the liposomes functionalized with HER under the same experimental conditions, the cell viabilities in SKBR-3 (HER+ breast cancer) cells and MDA-MB-231 (triple-negative breast cancer) were 27.4 ± 0.260 % and 40.1 ± 0.216% (p-value= 7.53×10^{-7}), respectively. Thus, it is suggested that coupling US with active targeting elicits synergistic effects and enhanced drug uptake by the cells. Also, liposomal treatments, i.e., control and targeted, along with US exposure, showed more pronounced effects in both cell lines, as the observed cell viabilities were significantly less than in control non-sonicated cells. The results presented in this thesis show promise of utilizing targeted liposomal delivery and ultrasound in the treatment of cancer.

Keywords: ***Drug delivery, Human Serum Albumin, Herceptin, MTT, immunoliposomes, ultrasound***

Table of Contents

List of Figures

List of Tables

List of Abbreviations

BCA - Bicinchoninic Acid Assay

DDS - Drug Delivery System

DLS - Dynamic Light Scattering

DOX - Doxorubicin

DPPC - Dipalmitoylphosphatidylcholine

EPR - Enhanced Permeability and Retention

FDA - Food and Drug Administration

HeLa - Henrietta Lacks cell line

HER - Herceptin

HER2 - Human Epidermal Growth factor receptor 2

HSA – Human Serum Albumin

mAb - Monoclonal Antibody

MI - Mechanical Index

MCF-7 - Michigan Cancer Foundation-7

MDA-MB-231 - M.D. Anderson - Metastasis Breast cancer- 231

NP - Nanoparticles

PBS - Phosphate Buffer Saline

PEG - Poly-ethylene Glycol

RES - Reticuloendothelial System

SDDS - Smart Drug Delivery System

SKBR-3 - Sloan–Kettering Breast Cancer-3

US - Ultrasound

Chapter 1. Introduction

1.1. Overview

Cancer refers to uncontrolled cell division due to DNA mutations. It occurs when proto-oncogenes are permanently activated by a mutation, turning them into upregulated proto-oncogenes, known as oncogenes; hence inducing the over-proliferation of cells [1]. Cancer can potentially spread throughout the body and form carcinomatous tissues known as tumors. As cancer progresses, it imposes an economic burden on countries because of the exorbitant treatment-associated costs. According to the 2018 World Health Organization (WHO) statistics, cancer is the second cause of death globally [2], preceded by cardiovascular diseases (CVDs) as the number one leading cause [3].

Through their normal life cycle, cells divide controllably, differentiate, and eventually die by the programmed cell death mechanism known as apoptosis. However, when cells sustain changes on a genetic and epigenetic level, they transform into cancer cells in a process called carcinogenesis [1]. Perturbing the ordinary growth path of the cells introduces behavioral changes. One way these genetic alterations are most often present is as gain-of-function (GOF) or loss-of-function (LOF) mutations [4].

To elucidate, GOF mutations affect proto-oncogenes, which under normal conditions, regulate the functions of cell proliferation, growth, and survival. However, during carcinogenesis, these mutant proto-oncogenes become overactivated and stop responding to regulatory mechanisms, leading to cellular over division. On the other hand, LOF mutations affect tumor-suppressor genes, which would normally regulate proto-oncogenes and keep cellular growth mechanisms in check.

GOF and LOF mutations together tend to increase growth potential, while simultaneously turning off growth regulatory mechanisms. These changes in function are often the result of DNA repair errors. As cells replicate their DNA, proteins encoded by repair genes check and correct any errors to prevent disease and cell death [4]–[6]. Hence, missed errors, which are the result of a faulty repair system, may be detrimental to cellular function. Moreover, as cancer cells replicate, they pass these errors to their daughter cells, leading to a poorly differentiated and genetically unstable cluster of cells.

Tumors resulting from the aberrant cell divisions can be broadly classified into benign, premalignant, and malignant tumors [7]. Benign tumors are cellular over-proliferation that are well-differentiated and localized and are not considered cancerous. Premalignant tumors, on the other hand, are localized but have the potential for malignant spread and do exhibit cancer-similar properties. Malignant tumors, also referred to as metastatic, are generally poorly differentiated and may spread to near and distant sites.

As a tumor undergoes rapid, chaotic growth, it exhibits a disorganized vascular network and becomes hypoxic due to insufficient oxygen supply. Tumor cells can secrete growth factors to induce vascularization to resolve this hypoxia and get nutrients from neighboring healthy cells by a process referred to as angiogenesis [6], [7].

Enduring research efforts have been intensive towards exploring potential technological advances in cancer therapy modalities. There are standard treatment approaches, as well as emerging novel ones. Immunotherapy is a treatment in which the patient's immune system is stimulated or artificially improved to fight cancer [8]. Also, targeted therapy, a branch of molecular medicine, is one of the treatments in which agents are directed to disturbing the cancer cells' inner working and pathways; hence it is deemed unharmful to the neighboring healthy cells [9].

For instance, the monoclonal antibodies Ramucirumab and Bevacizumab have shown effectiveness in blocking Vascular Endothelial Growth Factor (VEGF) receptors, thus inhibiting angiogenesis and, consequently, tumor growth [10], [11]. Surgery, radiotherapy, and chemotherapy are considered standard therapies and often used synchronously [8]. For instance, a patient can undergo radiotherapy to shrink the tumor before it is surgically removed and then undergoes a chemotherapy regimen(s) to complete the treatment cycle.

Radiation is one of the most well-established and commonly used treatments whereby high energy particles are used to bombard the diseased regions in order to damage the cells' DNA, preventing further division and growth [12]. In some cases, surgical intervention to remove the mass is imperative, which is then further examined by a pathologist who stages the cancer. The pathologist can also determine if the

resection margin is clear of tumor cells. If it is not, then surgery was not successful in entirely removing the mass, which significantly increases the risk of recurrence and might require further intervention.

Moreover, surgery is not only curative involving the extirpation of a tumorous mass but is also sometimes used as a diagnostic tool in biopsies [12]. As for chemotherapy, it is a systemic therapy that targets rapidly dividing cells by employing agents that interfere with the cells' life cycle. It is advantageous over surgery and radiotherapy in that it can act throughout the whole body, thus targeting cancer cells that metastatically spread far from the primary tumor site [13].

One of the most common chemotherapeutics used in the treatment of various cancers is the anthracycline agent Doxorubicin (DOX). As seen in Figure 1 [14], DOX is an amphiphilic molecule with a molecular weight of 0.6 kDa and a chemical formula of $C_{27}H_{29}NO_{11}$. Its cytotoxicity results from its primary mechanism of action, as it intercalates between the DNA nucleotides, disrupting topoisomerase II progression, an enzyme that uncoils DNA for transcription. The intercalation of DOX prevents the release of the DNA by topoisomerase II, ultimately halting DNA replication and eventual cellular division. Also, it is known to generate free oxygen radicals, which impair the cellular membranes of malignant cells and damage proteins and DNA [14].

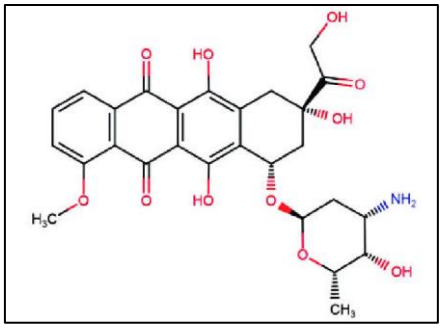

Figure 1: Chemical Structure of DOX [14]

Focusing on its physical and chemical properties, DOX is stable at acidic pH between 4.0-7.5, and it is photostable at concentrations above 500 µg/mL [15]. One alluring property of DOX is its intrinsic fluorescence, with excitation and emission spectra peaks at 480 and 590 nm, respectively [15]. It exhibits more fluorescence in hydrophobic environments, which makes it an optimal agent for use in drug delivery research. It is usually administered to patients via intravenous injections, either as a

continuous infusion or a single dose [14]. Although it is an effective anti-tumor agent, its side effects are most evident on cells exhibiting high division rates, such as hair follicles and the gastrointestinal tract lining; thus, hair loss, digestive tract ulcerations, vomiting, nausea, and diarrhea are all common complications/side effects [16]. Also, it has been known to induce cardiotoxicity by the upregulation of apoptosis receptors in cardiomyocytes [17].

Due to the detriment to the patients' quality of life and the potential lethality of some of the side effects associated with the common treatments, researchers and professionals are always venturing to find alternative novel therapeutic modalities to preserve the quality of cancer patients' lives. Such ventures aim at reducing the adverse side effects associated with the available therapies, as well as to have more targeted and efficient treatments.

Lately, Smart Drug Delivery Systems (SDDSs), which incorporate nanocarriers that have exclusive properties and specific bio-functions, have been gaining increasing attention because of their promising potentials and capabilities in targeted active drug delivery [18], [19]. Moreover, the release mechanisms of such systems are controlled and can be tuned to be stimuli-responsive to endogenous or exogenous triggers, such as pH, redox potential, temperature, electromagnetic waves, enzymes, ultrasound (US), and light. Some of the already well-established SDDSs include micelles, liposomes, polymeric nanoparticles, dendrimers, and magnetic nanoparticles [19].

1.2. Objectives and Statement of Purpose

This research is supplementary to the work of the Drug Delivery Research Group at the American University of Sharjah [20]. The group has worked on developing SDDSs incorporating liposomes as drug nanocarriers for the treatment of cancer, with a focus on ultrasound as the primary external release-triggering modality.

Untargeted liposomes, along with several surface-functionalized liposomes using different moieties, have been researched extensively. Synthesis, characterization, and release kinetics are all well-developed areas of the research, and recent efforts have been directed towards *in vitro* and *in vivo* analyses of the different liposomal formulations.

In vitro cell work of two types of targeted liposomes with ultrasound triggering is proposed in this study. The work particularly pertains to Herceptin- (HER), and Human Serum Albumin- (HSA) functionalized liposomes encapsulating DOX. It presents the synthesis, characterization, and *in vitro* analysis of the proposed DDS. To investigate the cellular uptake of different cell lines under the effects of US, the MTT assay is used, which examines the cells' metabolic activity and viability.

Chapter 2. Literature Review

2.1. Nanocarriers and Smart Drug Delivery Systems (SDDSs)

As previously defined, SDDSs are nanoplatforms with essential characteristics and bio-functions that make them optimal for the remote delivery of drugs to targeted sites under controlled release conditions. SDDSs overcome shortcomings of traditional treatment approaches, as they are designed to deliver appropriate dosages to specific anatomical locations, combat systemic side effects, prolong the circulation time of the drug and make it more bioavailable [18]. They incorporate nanoparticles (NPs) as drug delivery vehicles, which usually range in size from 1 nm to 800 nm. The synthesis routes of these NPs vary and are generally divided into chemical and biological ways, where the latter are preferred as they are safer and innocuous [19].

The morphologies of the NPs play a substantial role in the success of the SDDS. For instance, size and shape properties determine essential parameters such as circulation time, the efficiency of targeting, and internalization by the cells. The optimal size range for NPs is between 100 and 200 nm; as NPs exceeding 7 μm are expelled by the lungs, less than 6 nm are filtered by the kidneys, and between 0.1 to 7 μm are recognized by the reticuloendothelial system (RES) and phagocytized [21]. Moreover, regularly shaped NPs, as in spherical or cylindrical NPs, exhibit better performance than irregularly shaped ones, as the former are promptly internalized by the cells and move easily through the endothelial lining of the blood vessels. Likewise, surface functionalities such as hydrophobicity, charge, and targeting moieties can potentially alter the performance of the NPs [19], [21].

2.2. Passive and Active Targeting

Specific targeting and accumulation of therapeutics at the tumor site are of the main characteristics which give SDDSs their superiority. Once the nanocarriers are administered into the bloodstream, they should accumulate at specific anatomical sites and deliver the drugs precisely to the tumor cells/tissues, in order to reduce the side effects inflected on the healthy ones [13]. This targeting is achieved via three modes; passive, active (ligand), and triggered targeting [22]. Extensive research has established that the vascular structures formed by tumor angiogenesis are irregular, leaky, and defective.

Figure 2 [23] visualizes the difference between healthy and cancerous vasculature using fluorescence-tagged dextran administered intravenously into both types of tissues. In a normal vascular network, the blood vessels are regularly aligned, whereas, in the tumoral vascular network, the vessels suffer from size irregularities. Such faulty tumoral systems not only supply blood to the cancer cells, but they also aid in tumor metastasis and outspread by allowing the cells to escape into the bloodstream [24]. Moreover, the tumor's endothelial architecture lacks layers of smooth muscle and proper lymphatic drainage. Consequently, the tumor site suffers from poor fluid transport dynamics and mechanics.

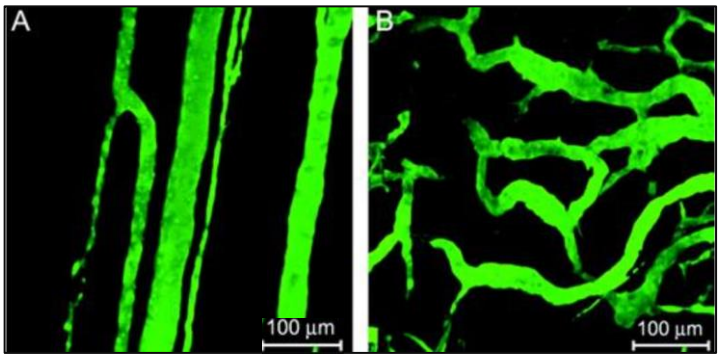

Figure 2: A) a normal vascular network where the vessels are parallel-aligned next to each other B) a tumoral vasculature with chaotic defective arrangement [23]

These features allow for the NPs to extravasate into the tumor's interstitium, and to accumulate in the disorganized neovasculature of these malignant tissues, in a phenomenon referred to as the Enhanced Permeability and Retention (EPR) effect as shown in Figure 3 [25]. EPR underlies the rationale behind passive targeting, which depends on the tumor's pathophysiological features and the unique bio-functions of the nanocarriers.

Some of the tumor-related factors to take into consideration when utilizing the EPR effect include, but are not limited to, tumor type and density, and its vascular permeability as a function of secretion of permeability factors. As far as the nanocarriers design is concerned, their chemical properties, surface functionalization, and charge, as well as morphologies, are all considerably impactful aspects [26].

However, designing SDDSs with complete dependence on passive targeting has significant limitations; such as the possible accumulation of the NPs in the spleen and liver as these organs have fenestrated vasculature, and the incapability of the NPs to

sufficiently penetrate deep enough through the complex tumoral network due to heterogeneities in structure [21]. Thus, the development of systems that incorporate both passive and active targeting mechanisms became imperative.

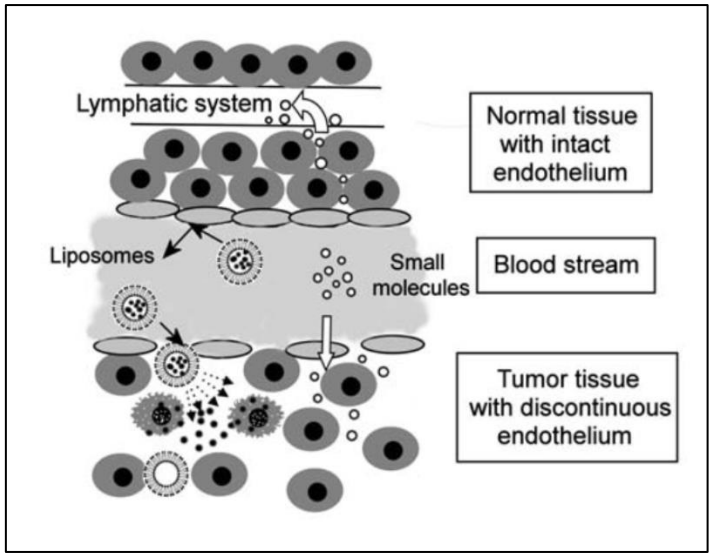

Figure 3: EPR enhances the accumulation of NPs due to poor vasculature [25]

Active-targeting can compromise the aforementioned inadequacies, as it depends on specific receptor-ligand interactions between highly expressed cell-surface receptors on the tumor cells and the engineered drug carrier's surface. NPs can be functionalized with ligands, or moieties, including proteins, antibodies, enzymes, vitamins and carbohydrates [19]. Since tumor cells are known to overexpress receptors that participate in growth and survival pathways, such receptors make promising active targets.

To this end, nanocarriers could be conjugated to the natural ligands of these receptors to ensure their accumulation and internalization at the tumor site [22]. Ideally, these receptors would be tumor neoantigens as these are overexpressed on tumor cells compared to healthy cells. Therefore, for this system to work, the ligand in question must have a high affinity to the target receptor in order to elicit a specific response, akin to a lock-and-key mechanism.

The mechanism of action of active targeting is based on receptor-mediated endocytosis; the drug enters the cytoplasm when the ligand bound to the receptor is engulfed by the plasma membrane, and then snipped into an endosome inside the cell as shown in Figure 4 [27].

The endosome provides an acidic environment which encourages ligand-receptor dissociation, releasing the drug and making it freely available for its pharmacological action to take place.

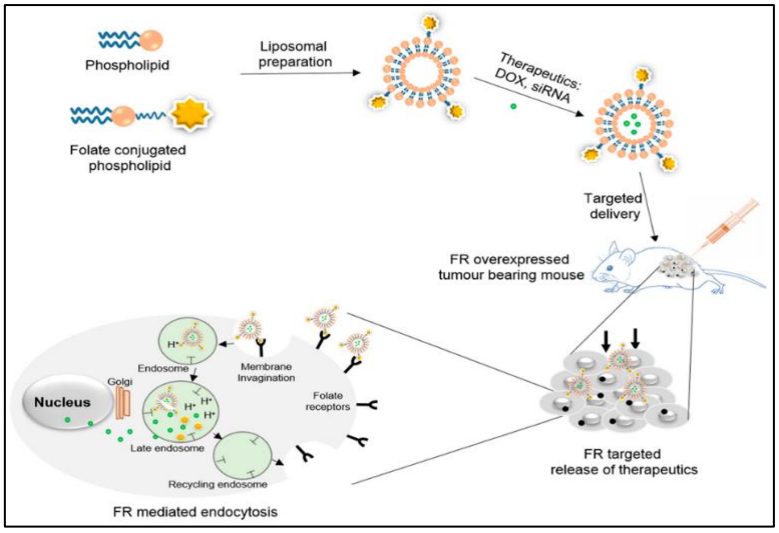

Figure 4: Example of active targeting where liposomes are decorated with Folic Acid (FA) as a ligand targeting the overexpressed Folate Receptors (FR) on tumor cells [27]

2.3. Nanoparticles (NPs) as Nanocarriers

State-of-the-art NPs is an area of research that has been heavily sought after due to its promising potentials in developing novel therapeutic modalities, that would overcome the insufficiencies of the currently available ones [21]. A promising nanocarrier is gold NPs, which consist of a gold core and are functionalized by the addition of a monolayer of ligands that assist in active targeting; they have distinguishing electrical and optical properties. *In vitro* experiments have shown their nontoxic and biodegradable potentials [19].

Also, ceramic NPs, such as Silica (SiO_2) and Zirconia (ZrO_2), are suited for numerous biomedical applications because they are inert, nonmetallic, highly abundant, and relatively inexpensive [19]. Polymeric NPs potentiate excessive exploitation due to their versatility in composition, structure, and properties.

There are synthetic, e.g., Poly Lactic Acid (PLA), and natural, e.g., Chitosan, based polymeric NPs, which are non-hazardous, biodegradable, stable, tissue-specific, and eco-friendly. They can be readily bio-functionalized to enhance their NPs-tumor interactions by polymeric coating or ligand binding [28]. Similarly, micelles have

competing applications in the biomedical field as they are biocompatible, physiologically stable, nontoxic, readily functionalized, and easily synthesized [29], [30]. Made up of amphiphilic molecules such as lipids or polymers, micellar systems self-assemble into well-intact structures when exposed to aqueous environments.

Governed by the "like attracts like" chemistry rule, the hydrophobic heads partition away from the aqueous environment allowing them to form hydrophobic cores, whereas the hydrophilic heads flank out in a brush-like shape. This will enable them to hide their hydrophobic cores inward while presenting their hydrophilic groups outward. Micelles have been established as successful SDDSs for cancer drugs like Paclitaxel, Doxorubicin, and cisplatin, among others [28].

2.3.1. Liposomes. Liposomes, which are the focus of this study, are nanosized to micro-sized drug carriers that resemble in their structure that of cell membranes. They have a lipid bilayer architecture comprised of cholesterol, phospholipids, and innocuous surfactants that assemble into concentric spheres with the inner and outer surfaces made up of the hydrophilic heads and the hydrophobic tails facing inwards; and hence shielded from the surrounding aqueous environment [28]. This distinguishing arrangement allows for the encapsulation of hydrophobic and hydrophilic drugs simultaneously, expanding the potential prospects of exploiting liposomes in the field of chemotherapeutics delivery [22]. Moreover, the encapsulated drugs are protected by the liposomes' physiological stability and biocompatibility; and are hence less susceptible to degradation and dilution upon administration. Figure 5 shows the different categories of liposomes based on their respective size, structure, and composition [32].

There exists a wide range of reproducible preparation techniques to synthesize liposomes, since they are becoming integral nanocarriers in many novel drug delivery systems. These systems are designed with the intent of targeting cancer, but also extend to serve other potential drug delivery applications. This is evident from the large expansion in the number of liposomal formulations recently present in clinical trials, as shown in Figure 6 [33].

Aside from the conventionally exploited large-scale liposomes production methods, such as the old extrusion method, electro-formation, double emulsions and

bubbling; researchers venture into alternative techniques that allow reproducibility, usability, stability, and enhanced process control [33]. A microfluidic technique proposed by Ota et al. [34] is based on transient membrane ejection, where a lipid bilayer is formed and then disturbed by a continuous fluid stream to form smaller vesicles, as shown in Figure 7.

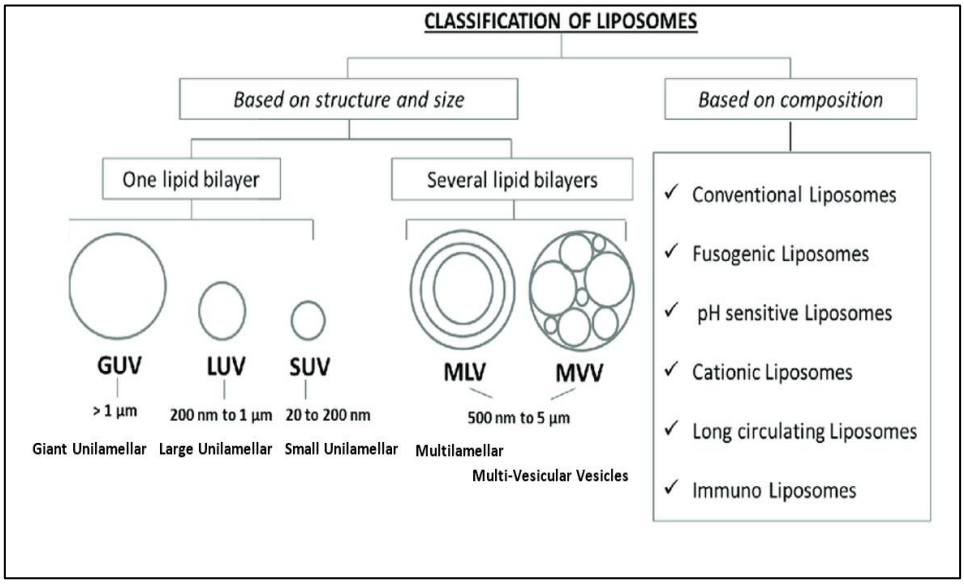

Figure 5: Classification of liposomes based on structure, size and composition [32]

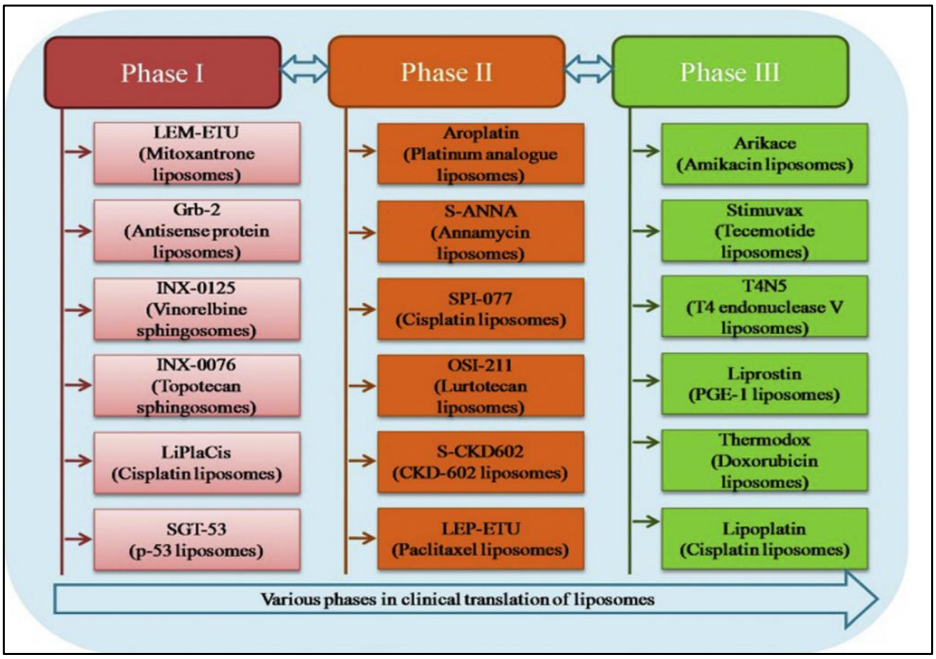

Figure 6: Recent liposomal formulations available in different phases of clinical trials [33]

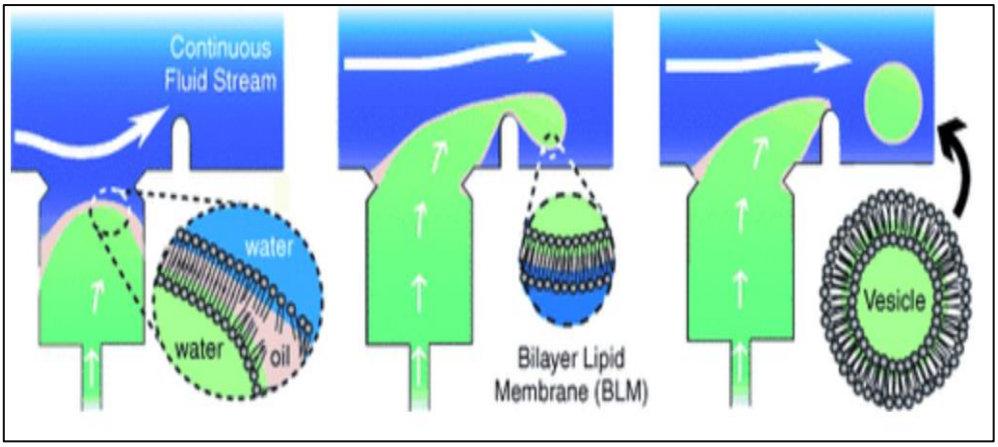

Figure 7: Formation of monodispersed unilamellar liposomes by the microfluidic technique [34].

Another technique established by Jahn et al. [35] involved the mixing of three streams where the central one contains phospholipids in alcohol encompassed by aqueous solutions, which form monodispersed liposomes. When the three streams are merged together in a microchannel, the alcohol diffuses into the aqueous phase, leaving behind the lipids to self-assemble into liposomes ranging in size from 50 to 150 nm.

Pautot et al. [36] developed another method where unilamellar bilayered liposomes can be formed by means of droplet emulsion transfer. The technique is based on forming a water-in-oil emulsion that is stabilized by phospholipids, where the droplets transfer to the aqueous phase. As the droplets move across the interface between the organic and aqueous phases, they gather another layer of lipids and form the liposomal structures.

Lastly, a technique established by Kastner et al. [37] depends on the chaotic advection of a staggered herringbone micromixer (SHM), where separate streams of lipids solution and aqueous buffer are injected into the device with controlled flow ratios. Over the surface of the channel, the fluid streams mix, stretch, and fold due to the chaotic advection, promoting mass transfer, which produces liposomes of controllable size and polydispersity Figure 8.

2.3.2. PEGylation. Prolonged circulation of the nanocarriers in the body to promote drug bioavailability is an aspect that has garnered substantial interest in the field of SDDSs. The half-life of the liposomes is a function of their size, composition, surface charge, and lipid saturation; and it is always desired to be improved to evade

rapid clearance [38]. However, the breakthrough in promoting prolonged circulation of the liposomes was through PEGylation, which enhanced surface stability and prevented liposomes from opsonization [25].

Opsonization is the tagging of the liposomes as foreign substances by the plasma proteins, leading to their consequent elimination by macrophages. The liposomes' surfaces can be engineered with stealth-imparting polymers such as PEG (polyethylene glycol) chains to shield them from immune recognition by the reticuloendothelial system (RES) and clearance by the mononuclear phagocyte system (MPS) [25].

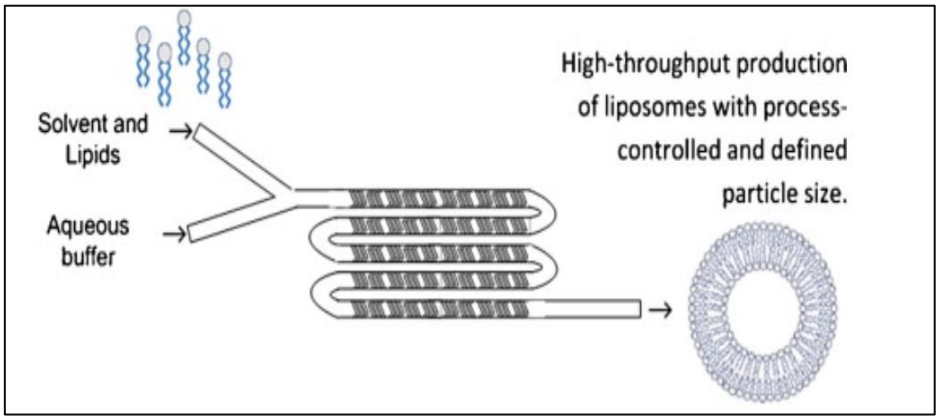

Figure 8: Staggered herringbone micromixer (SHM) for liposomes production [37]

The PEG chains, examples are shown in Figure 9 [25], are soluble in aqueous and organic solvents, highly biocompatible, easily synthesized, have a linear or branched structure, and show low immunogenicity. The chains can vary in length and configuration, and they are grafted into the liposomes through linkers to create the PEGylated liposomes, commonly referred to as stealth liposomes.

A study [38] claimed that optimum circulation times could be achieved by incorporating 5 mol% polyethylene glycol with a molecular weight of 2000 g/mol, PEG2000, into the formulation, and elaborated that the use of PEG2000 is "based more on tradition rather than scientific reasoning." The choice of the linker is essential, as it alters the extent to which the PEG chains are implanted into the liposomal membranes and can also impose behavioral changes to the liposomes. For example, phosphate linkages are suspected of provoking opsonization, while ester linkages, which are pH-sensitive, are vulnerable to biological decomposition [38].

A study [25] compared the *in vivo* pharmacokinetic performance of free DOX with PEGylated and non-PEGylated liposomal formulations. Interestingly, the PEGylated liposomal DOX clearance rate decreased by 100-folds (Cl= 0.023 L/h), and its half-life ($t_{1/2}$=83.7 h) was prolonged by 8-folds, compared to free DOX (Cl=25.3 L/h, $t_{1/2}$=10.4 h). Moreover, the distribution volume decreased significantly from 364 L to 139 L to 3.0 L in the free DOX, non-PEGylated, and PEGylated liposomal DOX, respectively. This conclusion demonstrated that PEGylation prevents premature drug release and that most of it remained entrapped without leakage.

Another study by Awad et al. [39] investigated the effects of PEGylation on the US-mediated release kinetics from calcein-loaded liposomes. This research concluded that the calcein (model drug) PEGylated liposomes were more sono-sensitive and presented significantly enhanced release profiles when exposed to pulsed US at 20 kHz. As shown in Figure 10, the release profiles of the PEGylated liposomes were higher than the non-PEGylated ones at all tested power densities. It was reported that the PEGylated liposomes released 57.5% ± 4.5 of their contents, whereas the non-PEGylated ones released only 22.7% ± 1.7 by the end of the third US pulse at the 12 W/cm^2 power density. The conclusions from this study further emphasize the effectiveness of PEGylation on enhancing the overall performance of the SDDS.

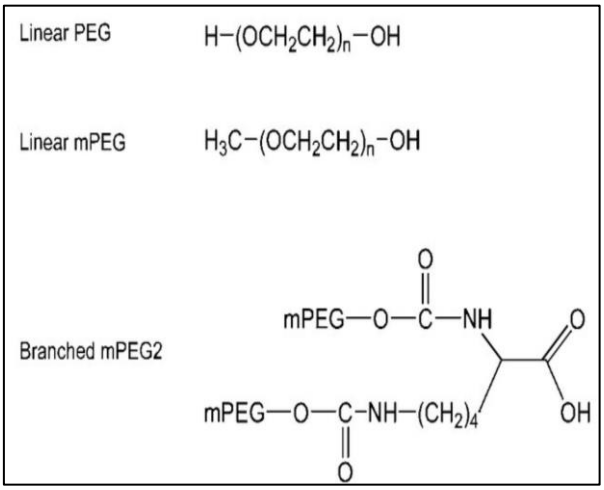

Figure 9: The structure of different PEG molecules [25]

2.3.3. Ligand-functionalization and active targeting of liposomes. Another engineering modification to improve the nanocarriers' cellular uptake and their accumulation at the desired anatomical site is functionalizing the surface with ligands

as briefly introduced earlier. Some of the actively targeted liposomal systems have reached clinical trials.

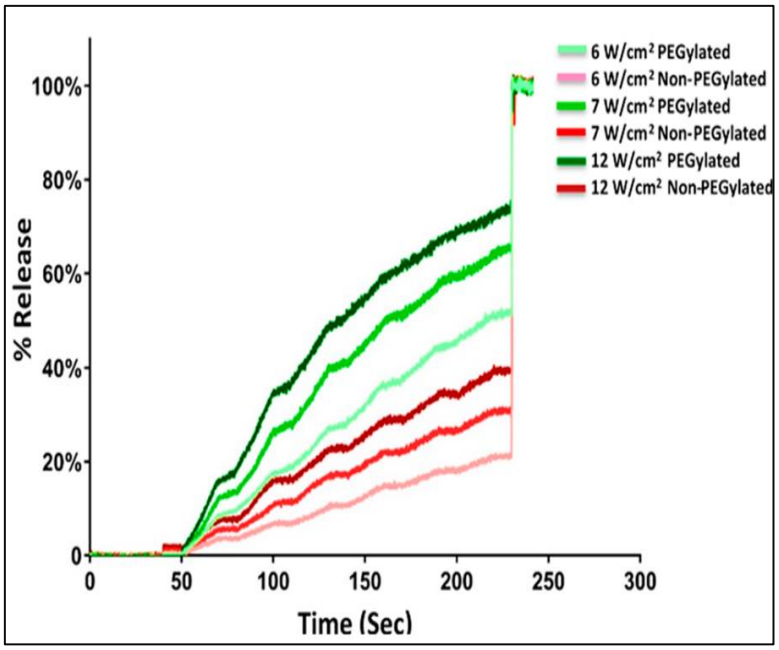

Figure 10: Release profiles of calcein-loaded PEGylated and non-PEGylated liposomes triggered by different US power densities [39]

For instance, DOX liposomes, functionalized with the monoclonal antibody GAH, for the treatment of metastatic stomach cancer, reached phase I [40]. It is necessary when functionalizing the liposomal surface with a ligand to ensure that the critical ligand density is not exceeded in order to avoid aggregation, which would hinder effective/sufficient binding. Also, the ligand of choice should exhibit a high binding affinity to the receptors and low immunogenicity.

Several other studies have shown the effectiveness of active targeting on liposomal systems [41], [42]. A study [43] investigated the *in vitro* performance of dual-targeted mAb-conjugated DOX-loaded liposomes on human B-cell lymphoma. The functionalizing of the liposomes increased their affinity and uptake and caused a 10-folds decrease in the IC_{50} value. Another *in vitro* study [44] using human cervical cancer (KB) cells and folate-conjugated calcein-loaded liposomes showed that the cellular uptake increased by 37-folds when the targeted liposomes were used.

Gabizon et al. [45] also used the folate ligand to investigate the *in vivo* performance of DOX liposomes on human cervical (KB) and murine lymphoma (J6456) cells. The targeted liposomes significantly inhibited tumor growth compared to

the nontargeted liposomes. The two ligands pertinent to this work are Human Serum Albumin (HSA) and Trastuzumab, the latter commercially known as Herceptin.

2.3.3.1. ***Human Serum Albumin (HSA) targeted liposomes.*** HSA is a multi-functional protein that is synthesized in the hepatocytes and is abundantly found in the plasma. HSA has a high affinity to hydrophobic molecules, and its half-life extends to 19 days before it gets catabolized by skin and muscle cells [46]. Functionally, it acts as a carrier protein for other substances, contributes to maintaining the osmotic pressure and blood pH levels, and has antioxidant properties. Moreover, it is an important prognostic biomarker, as its levels decrease in times of systemic inflammation such as cancer [46]. Studies[47], [48] have shown an overexpression of HSA receptors, i.e., heterogeneous nuclear ribonucleoproteins (hnRNP), on breast cancer cells.

Yang et al. [49] concluded that heterogeneous nuclear ribonucleoprotein M (hnRNPM) is overexpressed in MCF-7, MDA-MB-231, KPL-4, and 7T4D cell lines. Figure 11, red-bordered, represents *in vivo* xenografts of MCF-7 tumor cells, which indicate that hnRNPM promoted tumorigenesis. It is noticeable from the tumor volume that the effect of the upregulation and overexpression of the hnRNPM inhibited cell apoptosis, enhanced cell viability, and promoted tumor growth.

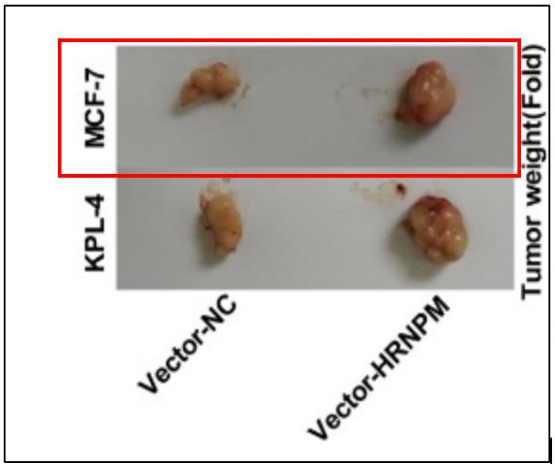

Figure 11: In vivo xenografts of MCF-7 tumor cells [49]

Motevalli et al. [50] investigated the co-delivery of Curcumin (Cur) and DOX via Albumin nanoparticles (ANPs) to MCF-7 cells. Figure 12 shows confocal laser scanning microscopy images that illustrate the drug uptake by untreated cells, cells treated with Cur-ANPs for 1.5 hours then followed by DOX-NPs treatment for 1.5

hours, and cells treated with the Cur-DOX-ANPs for three hours. LTR, lysotracker red, is a fluorescent tracker to label lysosomes inside cells. The study concluded that the Albumin functionalized NPs, along with co-delivering both chemotherapeutics, yielded the highest drug efficacy. The results were further supported by an MTT assay, which suggested that the cell viability decreased as the drug concentrations increased, independent of the followed treatment regime (simultaneous co-delivery or subsequent administration).

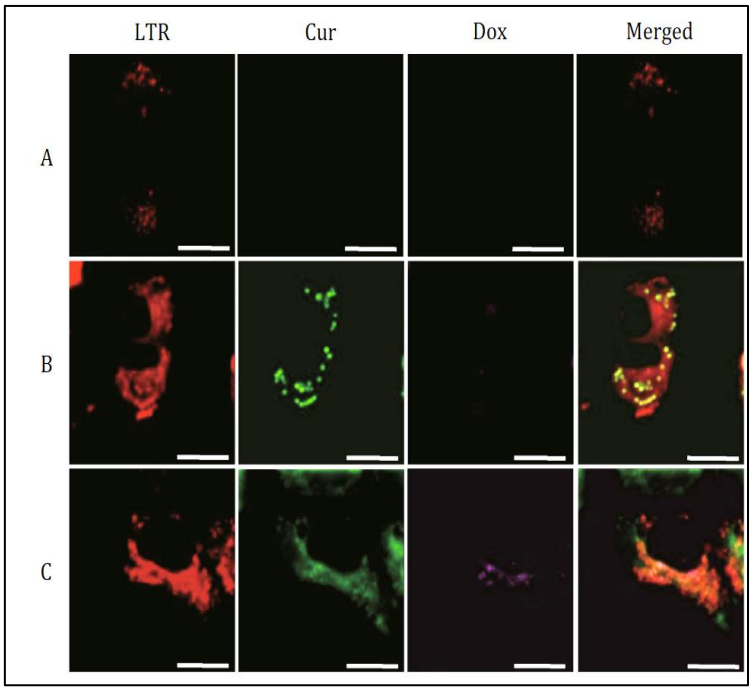

Figure 12: Confocal laser scanning microscopy images of MCF-7 response to different ANPs treatments. A) untreated cells B) pretreated cells with Cur then DOX C) concurrently treated cells with Cur and DOX [50]

2.3.3.2. *Herceptin targeted liposomes.* Herceptin (HER), also known as Trastuzumab, a monoclonal antibody, is a lab-made protein that targets overexpressed human epidermal growth factor receptors (HER2). In almost 25% of breast cancer cases, the HER2 receptors are found to be overexpressed 1000 times more than on healthy cells [51].

The Human Epidermal Growth Factor Receptor family includes four transmembrane Tyrosine kinase receptors, but HER2 is of particular interest because it lacks a known ligand and is found to be homogenously distributed within the tumor [51]. Herceptin is also used on its own as a therapeutic agent alongside chemotherapy, as a means of immunotherapy.

Vu et al. [52] showed that combining Trastuzumab with chemotherapy in an adjuvant setting produces enhanced response rates compared to chemotherapy alone. Although the exact mechanism of action of Herceptin is not fully understood, the study proposed three mechanisms by which it acts: HER2 internalization and degradation, Antibody-dependent cellular cytotoxicity (ADCC), and the inhibition of the MAPK and PI3K/Akt pathway, which leads to arresting the cell cycle. However, clinical benefits are mostly attributed to the immune cell-modulated activity of trastuzumab, as several studies [53]–[55] have shown that natural killer cells target the HER2-overexpressing cancer cells that are coated with the drug Herceptin.

Collins et al. [55] studied the effects of trastuzumab in inducing ADCC on different cell lines, ones that overexpress HER2 and others that do not. The laser scanning confocal images of the drug attached to the HER2 receptors can be seen in Figure 13, and it is obvious how there is more drug bound to SKBR-3 and T47D cells because they overexpress the receptors, whereas the rest of the cell lines do not. The study concluded that the cell lines which overexpress HER2 showed increased ADCC effects upon treatment with the drug, whereas less drastic effects were observed in the HER2-negative cell lines.

Chen et al. [56] carried out an MTT assay to investigate the inhibition to proliferation effects of 3 different concentrations of Herceptin (5, 15, 20 μg/ml) on SKBR-3 cells and the triple-negative HCC-1937 cells. The researchers also varied the post-treatment incubation period between 24 hours, 48 hours, and 72 hours. As shown in Figure 14, the SKBR-3 cells experienced most inhibition to proliferation when incubated for 72 hours at a drug concentration of 20 μg/ml, and a clear time-dependent dose-effect relationship can be drawn.

As for the effects on the triple-negative cell line, the inhibition percentages due to Herceptin were minor compared to those on the HER2-overexpressing cell line. Also, it can be observed that insignificant differences appear when comparing the 10 μg/ml and 20 μg/ml concentrations, regardless of the incubation times. Thus, the benefits of treating cell lines with trastuzumab, where HER2 expression is non-amplified, are considered limited. There has been extensive research that attested to the efficacy of actively targeting overexpressed HER2 receptors using Herceptin as a targeting moiety. Such liposomes bound to monoclonal antibodies, are known as

immunoliposomes. A study by Kirpotin et al. [57] evaluated the *in vitro* performance of PEGylated versus non-PEGylated Rhodamine-loaded liposomes targeted with Fab‘ (fragment antigen-binding) fragments of rhuMAbHER2, on human breast cancer (SKBR-3 and BT-474) cells, where the former showed amplified cellular binding and internalization.

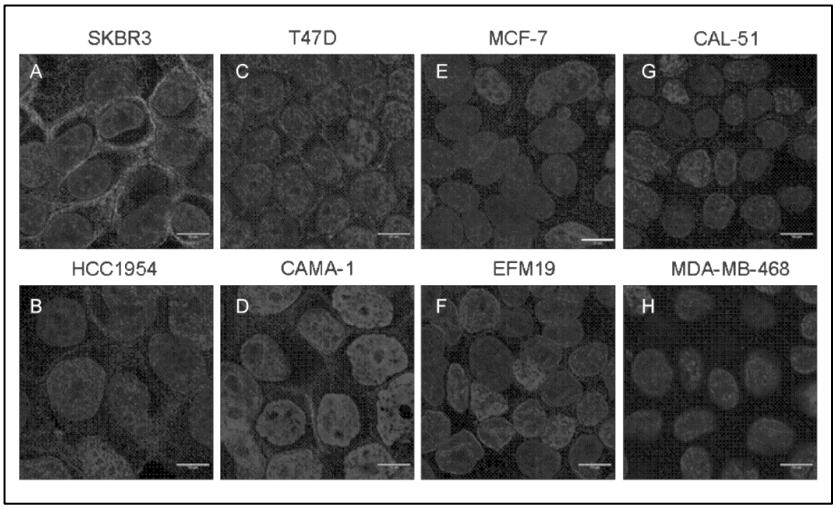

Figure 13: Laser scanning confocal images of Herceptin bound to HER2 receptors on different cell lines [55]

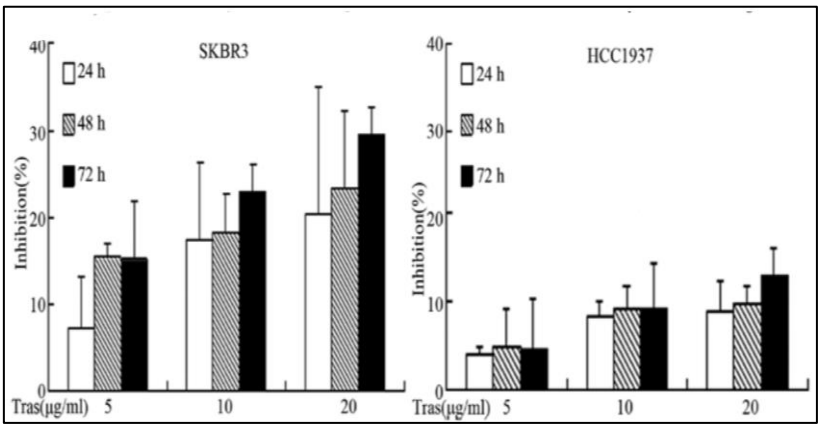

Figure 14: Inhibition to cell proliferation in SKBR-3 and HCC-1937 cells for different concentrations and different incubation times [56]

A similar study by Park and co-workers [58] investigated the performance of DOX-entrapped anti-HER2 immunoliposomes on human breast xenografts (BT-474, MCF7, MDA-MB-453) cell lines. The results showed that the immunoliposomes overall cure rates reached 16%, whereas free and unconjugated liposomal DOX showed no cures.

Two other studies targeted HER2 with DOX loaded immunoliposomes and studied their *in vivo* effects on human breast cell lines (BT-474 and SKBR-3). Laginha et al. [59] showed that the increase in cellular uptake of the immunoliposomes increased by 2-folds compared to the nontargeted liposomes and by 20-folds compared to free DOX.

Likewise, Bandekar et al. [60] showed a significant 160% decrease in the tumor volume when treated with the DOX-immunoliposomes as opposed to the nontargeted ones. Thus, it is concluded that actively targeting the overexpressed HER2 receptors does indeed enhance the DDS's overall performance and improve the cellular uptake and therapeutic efficacy of the drug.

2.4. Ultrasound (US) as a Triggering Mechanism

Upon injection into the patient's bloodstream, the nanocarriers tend to accumulate and pile up at the tumor's leaky vasculature due to the before-mentioned EPR effect. In order to unleash the full potential of these drug-loaded vehicles, it is mandated to utilize a triggering mechanism in order to release the encapsulated drug in a controlled, timely, and efficient manner.

Ultrasound has gained considerable attention in research as one of the best drug release mechanisms due to its noninvasiveness, safety record, and relatively low costs. Although it is best known in the medical field for its imaging application, i.e., embryos monitoring and imaging, it has developed to become a means of diagnostics and therapies.

The US's mechanism of action relies on its waves. US waves are longitudinal mechanical sound waves that require a medium for the energy to be transmitted. Transducers contain piezoelectric crystals that produce acoustic waves as an alternate electrical current is converted into mechanical energy. When an electric pulse is generated and sensed by the crystal, it vibrates; consequently, the surrounding medium experiences pull and push forces, and thus waves are generated [61].

The four main parameters that define US waves are frequency, intensity, attenuation, and the mode of operation [62]. Frequency is defined as the number of full waves that pass per second, and is measured in Hertz (Hz). This parameter determines the depth of penetration of the waves and their ability to induce cavitation events. Power

intensity is usually measured in Watts per centimeter squared (W/cm^2), and it quantifies the amount of power, or the energy, delivered to the tissues per unit area [62].

Increasing the intensity of US alone could cause cell death if it is applied continuously, as Wang et al. [63] reported when he used tested 1.1-MHz US at two different intensities on K562, a myelogenous leukemia cell line. Results showed that cell death increased to 14% at an intensity of 1 W/cm^2 and to 40.7% at an intensity of 2.1 W/cm^2. Attenuation accounts for the losses due to the dissipation of energy in the tissue, or medium. As for the mode of operation, it describes the manner by which the US is applied, whether continuous or pulsed, and whether focused or unfocused. It is noteworthy to mention that a higher frequency indicates a shorter wavelength, thus shallower penetration, which leads to more losses and higher attenuation [64]. These parameters must be carefully tuned and considered when designing a drug delivery system in order to guarantee its success.

There are two main mechanisms by which US impacts cells and tissues in therapeutic applications, i.e., thermal and mechanical effects [61]. Thermal effects are experienced by sonicated tissues due to hyperthermia, whereby exposed tissues experience an overall increase in the medium's temperature.

The extent to which the medium absorbs energy is a function of multiple factors, such as the frequency of the US and the exposure time. Moreover, some factors are intrinsic to the medium itself, such as its absorption coefficient, the higher the value of this coefficient, the more thermal effects will be experienced by the tissues [61].

The effect of US on drug release from liposomes is a well-developed area of research [65]–[67]. When the acoustic waves interact with liposomes, some of the acoustic energy will be dissipated and absorbed by the phospholipid bilayer, causing an increase in temperature, which in turn slightly liquifies the microstructure of these nanovehicles and promotes drug release.

In drug delivery applications and to achieve hyperthermia, the temperature in the tissues should not exceed 43 °C. Within a temperature range of 40 to 43 °C, the increase in temperature accompanied by an increase in blood flow causes vasodilation as well as an increase in the permeability of the tumor's vasculature, hence enhancing the accumulation of nanoparticles at the diseased site. However, strong hyperthermia,

which occurs when temperatures increase beyond 43 °C, could cause necrosis to both healthy and cancerous cells and can cause severe burns, as shown in Figure 15 [64].

The other mechanism by which US induces biological effects is mechanical, mainly through cavitation events. Bubbles pre-exist or are generated in the fluid due to the pressure dropping below the liquid's vapor pressure. The pressure drop could be induced by exposure to US waves.

Acoustic cavitation occurs when these cavitation nuclei, which are gas-filled bubbles in the insonated liquid media form, grow, oscillate, and eventually collapse [68]. It has two primary modes; stable, or non-inertial, and inertial, or collapse, as shown in Figure 16 [31].

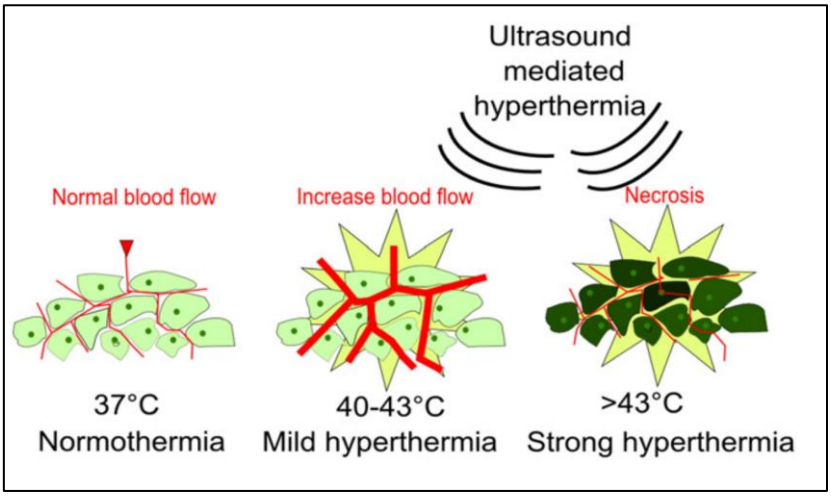

Figure 15: Thermal window for therapeutic hyperthermia [64]

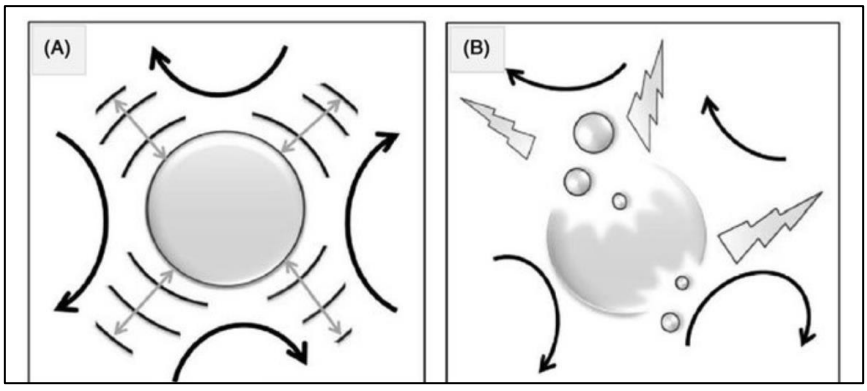

Figure 16: A) stable cavitation where the microbubble oscillates in response to acoustic pressure within equilibrium range B) collapse cavitation where the microbubble exceeds its resonance size thus collapse and produce microstreams and cavitation nuclei [31]

As suggested by the name, in stable cavitation, the bubble would expand and contract within its equilibrium range, in response to the shifting of the US waves' pressure from positive to negative and vice versa. However, it would not rapture or break. On the contrary, collapse cavitation occurs when the bubble does not endure the fluctuations of the waves' crests and troughs.

Thus, it goes through a contractile stage where it hastily grows to up to three-fold its resonance size and then collapses aggressively [68]. US exposure could be achieved by placing the samples in a sonication bath, or by placing a sonicating probe into the sample as shown in Figure 17 [39].

The rapid growth in bubble size is due to rectified diffusion, where more gas diffuses into the bubble than diffuses out. As a result of the bubbles' collapse, local surges in temperature and pressure are observed. Subsequently, microstreams and shock waves are also generated, which disturb nearby cells and tissues. It is believed that this is the main mechanism by which release from nanocarriers is induced, due to exposure to US waves [22], [68], [69].

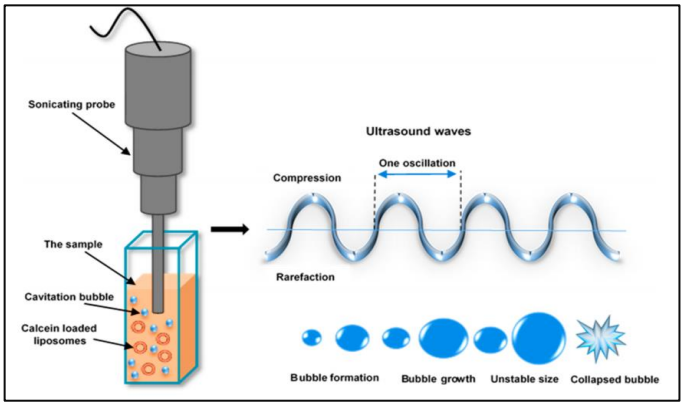

Figure 17: a schematic illustrating induction of collapse cavitation due to US waves [39]

Husseini and Pitt [70] proposed that the shearing of the micelles in the vicinity of shockwaves caused the release of DOX from Pluronic P105 micelles, as their structure got disturbed and destroyed Figure 18. Therefore, the same conclusion can be extended about the effects of US on inducing release from other lipid-based nanocarriers.

Apfel and Holland [71] proposed the calculation of a Mechanical Index (MI), which measures acoustic power and serves as a reasonable indicator of the US's ability

in inducing cavitation-associated bioeffects. It is calculated by dividing the peak negative pressure of the US beam by the square root of its center frequency, where a MI greater than 0.3-0.4 is considered sufficient to initiate transient cavitation events in the insonated media. According to the FDA, a MI of 1.9 is the allowed threshold for the safe nondamaging application of US, beyond which, occurrences of micromechanical damage are imminent [72].

A specific phenomenon of transient cavitation occurs when the bubbles are bounded by any given biological boundary from one side, while the other side oscillates freely, it is referred to as asymmetric collapse. The bursting bubbles do not generate a regular shock wave that propagates in spherical dimensions, but rather the energy from the collapse is directed inwards towards the center of the bubble from the free side propagating linearly. This non-spherical collapse induces high-speed energy-intensive acoustic microjets. The shock waves, along with the shooting microjets, can cause neighboring liposomal membranes to burst open, thus promoting drug release [64].

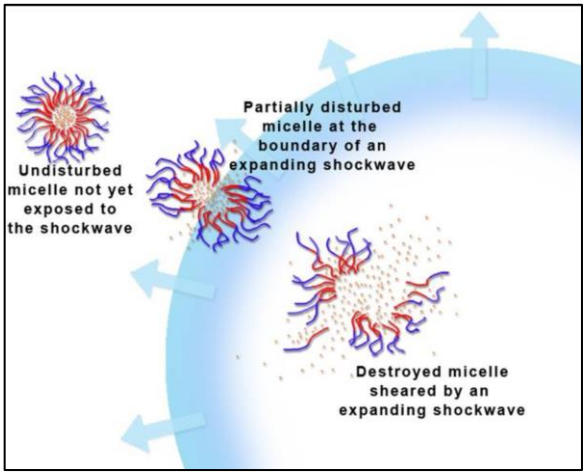

Figure 18: Proposed mechanism of DOX release from Pluronic micelles due to shearing effects [70]

Similarly, if the bubbles happen to be close to the tumor site, their collapse can induce the formation of pores in the plasma membranes of the cells in a process called sonoporation [73]. This further enhances the accumulation of the drug at the tumor site. When considering the application of US in drug delivery, collapse cavitation has a more predominant role compared to stable cavitation. The former has been shown to enhance drug uptake, and the payload delivery to the individual cells as their permeability is

altered with the aid of shock waves and microjets. In contrast, stable cavitation has some effects on changing the overall permeability of diseased vessels.

The other mechanical effect of US is an acoustic radiation force, which occurs when operating at a frequency in the MHz range [62]. Acoustic streaming happens when US generates forces due to large-scale convective motions of the fluid's body, which indirectly pushes the nano-carriers into the tumor's vascular walls, thus prolonging their retention time. Also, US can create shear forces that widen intracellular spaces between the cells leading to the same result of enhancing penetration and retention of the nanoparticles [61], [62]. According to Husseini et al. [68], acoustic streaming barely contributes to the mechanisms by which US triggers release because fluid convection is already quick to be altered by the ultrasonic beam in the body's vascular system. Generally, mechanical, along with thermal effects, suggest that US is one of the best drug delivery triggers, as it is considered safe, non-invasive, and does not affect healthy cells.

2.5. The MTT Assay

One of the well-established assays to test for cellular metabolic activity is the MTT assay, which was first introduced by Mosmann in 1983 [74]. It is a versatile quantitative colorimetric assessment that is used to quantify cell growth and viability, measure cytotoxicity, assess growth-inhibiting agents as well as study cell proliferation and activation under specific conditions. The mechanism of action by which the assay works is based on the reduction of 3-(4,5-dimethylthiazol-2-yl)-2,5-diphenyltetrazolium bromide, referred to as yellow tetrazolium salt and abbreviated as MTT, to formazan crystals. This metabolic reaction, shown in Figure 19, occurs in the mitochondria of the living cells by the action of oxidoreductase enzymes, which actively cleave MTT and reduce it to formazan [75].

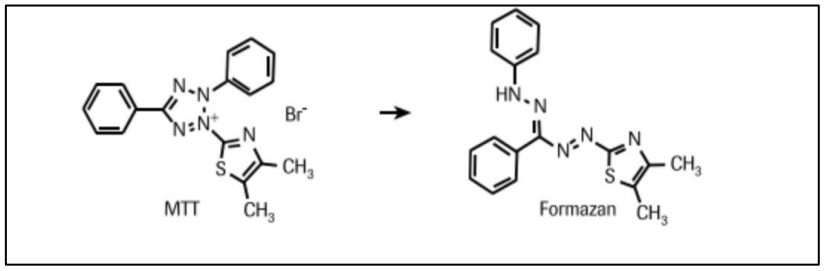

Figure 19: Reduction of MTT salt to formazan crystals [75]

The formazan crystals are purple in color and are partially insoluble in the media. Thus, they have to be dissolved by a solubilization solution prior to measuring the absorbance using a spectrophotometer. An approximation of cell viability can be deduced by the color in the wells, as darker shades of purple indicate more metabolically active cells. Figure 20 shows one of the plates used in this study, and different shades indicate the variations in cell viability. The absorbance wavelength of the dissolved formazan ranges from 500 to 600 nm [75].

The MTT assay is advantageous because it is rapid, provides precise results, and is also convenient for analyzing multiple samples at once. Moreover, Mosmann [74] demonstrated that the assay has broad applicability because all the tested cell types in his study formed formazan crystals upon the cleavage of the MTT by the alive cells. The detailed protocol followed in this research is found in the methodology section.

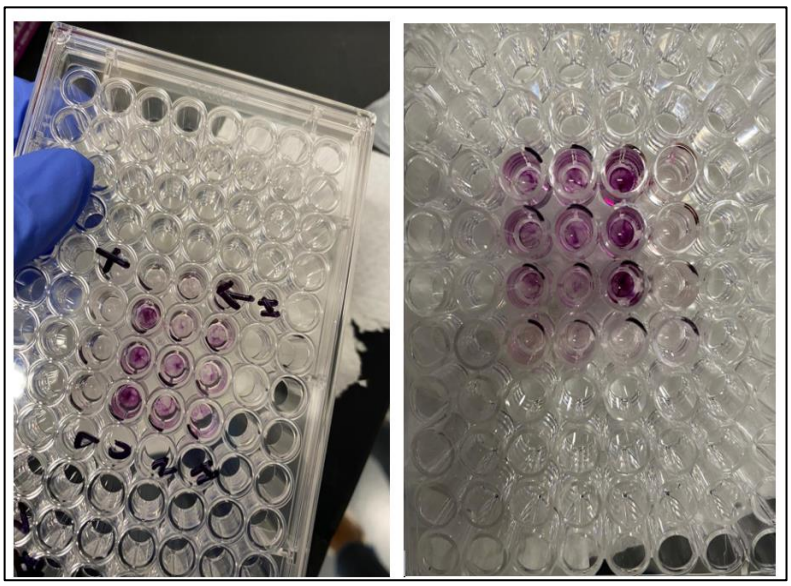

Figure 20: MTT 96 well plate HER-DOX batch.

2.6. Relevant *In Vivo* and *In Vitro* Studies

Pitt et al. [76] compared the effects of DOX-loaded liposomes on BDIX rat-bearing rat colonic carcinoma. The drug efficacy in the mice, which were exposed to the liposomal treatment with sonication at 20 kHz for 15 minutes over a 4-week period, was significantly enhanced compared to the control group.

Another study [73] suggested synergism between US when combined with the drug upon the exposure of HL60 cells to US at 255 kHz for half a minute; the plasma

membranes of the cells exhibited pores (sonoporation) from which the cytoplasm was extruding. However, when the cells were exposed to US alone without the drug, the same observation was not evident. Similarly, Saito et al. [77] reiterated that US enhances the permeability of cell membranes upon exposure to US with the drug, as tested on corneal endothelium cells. Another two related studies by Rapoport et al. [78] and Munshi et al. [79] investigated the effect of sonication on the uptake of the DOX and its IC_{50} value on HL60 cells. The first study found, by means of fluorescence, that after an hour of insonation at 67 kHz and 2.5 W/cm^2, the amount of DOX that reached the cells' DNA has significantly increased [78]. The second study found out that the IC_{50} value decreased significantly upon sonication for an hour at 80 kHz [79]. It is noteworthy to mention that both studies were carried out at a constant temperature of 37 °C, to eliminate any effects of hyperthermia.

Furthermore, Yuh et al. [80] carried out an *in vivo* study on mice bearing SCC7, murine squamous cell carcinoma. The experimental group treated with DOX-liposomes accompanied by pulsed high-frequency US (HFUS) exhibited 124% more drug accumulation at the tumor site, as opposed to the control group, which received the DOX-liposomes treatment without exposure to US. Lastly, a study by Thomas and co-workers [81] investigated the phenomenon of microbubbles cavitation aided by US exposure in triggering the DOX release from liposomes to EGFR overexpressing tumors. MDA-MB-468 xenografts were used to conduct the *in vivo* analysis, and it was found out that the ultrasound-mediated cavitation of microbubbles increased the drug uptake by 66% in the tumor.

Several *in vitro* analyses were carried out to illustrate the effects of US exposure and active targeting on the efficiency of the DDS. A study by Salkho et al. [82] examined the *in vitro* performance of US-triggered estrone-targeted liposomes for breast cancer treatment and assessed the induced drug release profiles under exposure to LFUS (low-frequency US) and HFUS (high-frequency US). It was reported that conjugation of estrone to the liposomes significantly enhanced their cellular uptake by estrogen overexpressing MCF-7 cells (ES+ cell line) than by MDA-MB-231 (ES- cell line) (p-value= 6.98×10^{-4}). Moreover, results of the flow cytometry on MCF-7 cells showed that the calcein accumulation increased by 70% upon exposure of the cells to US, for 60 seconds of pulsed sonication in a 40 kHz bath Figure 21.

Furthermore, it was concluded that varying the power density of the US stimulus had significant effects on the release profiles. Figure 22 shows calcein release profiles from estrone-targeted liposomes, triggered at a frequency of 1.07 MHz and a power density of 10.5 W/cm^2 (blue), 1.07 MHz and 50.2 W/cm^2 (green), and 3.24 MHz and 173 W/cm^2 (red). As the power density increases, the nanocarriers released more of their contents; due to the augmented shearing and cavitation effects of the waves on the nanocarriers. The study concluded that functionalizing the liposomes did not significantly alter their release kinetics and that synergistic effects exist when receptor-mediated targeting is combined with US.

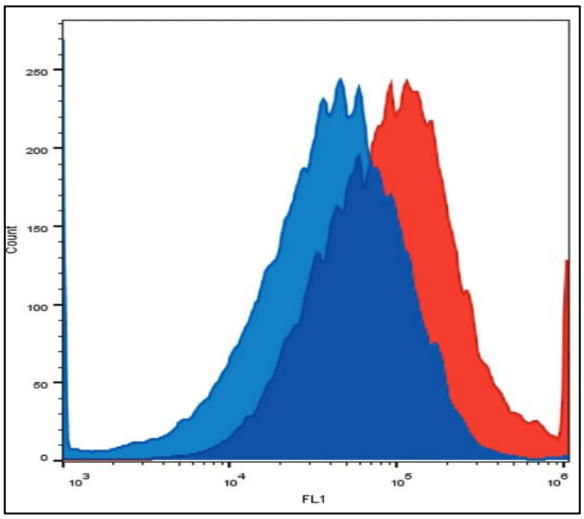

Figure 21: Flow cytometry histogram showing calcein uptake by MCF-7 cells with (red) and without (blue) exposure to pulsed US [82]

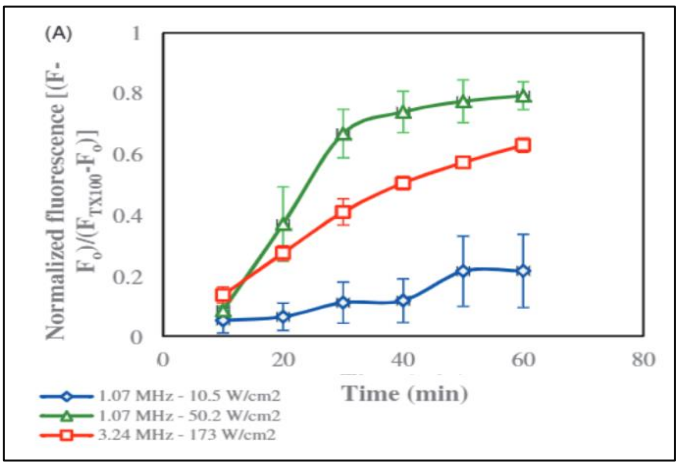

Figure 22: Calcein release profiles from estrone-bound liposomes at different power densities of HFUS [82]

A similar study by Awad and co-workers [83] investigated the intracellular model drug uptake encapsulated in PEGylated HSA-conjugated liposomes in MDA-MB-231 and MCF-7 (breast cancer cell lines) versus the uptake in HeLa (a cervical cancer cell line); where the former overexpress albumin receptors on their surface. Flow cytometry results indicated that the uptake of the model drug calcein was significantly higher in the breast cancer cell lines as opposed to the human cervix carcinoma cell line, confirming that functionalizing the liposomes' surface with HSA as a ligand had enhanced its binding affinity and active uptake via mediated endocytosis due to its receptors overexpression on the MDA-MB-231 and MCF-7 cell lines.

It is reported that the geometric means of the average uptake of the drug in the HeLa cell lines treated with control liposomes and PEG-HSA liposomes were 2773 ± 110 and 2885 ± 435, respectively; indicating no statistical significance in the cellular uptake due to HSA conjugation. Furthermore, fluorescence data showed that the cellular uptake of the model drug from the PEGylated HSA liposomes was significantly higher compared to the control liposomes, where the uptake increased by 84% in the MDA-MB-231 and by 90% in MCF-7 cell lines. The uptake was further significantly increased upon exposure to US at 40 kHz to reach up to 155% and 175%, respectively, in the MDA-MB-231 and MCF-7 cell lines.

Another study carried out by Okamoto et al. [84] used a tumor spheroid 3-dimensional cell culture model in order to get a closer simulation of the actual tumors' microenvironment and complex network. They observed that bovine serum albumin-(BSA-) bound Paclitaxel (PTX) encapsulated liposomes had significantly inhibited cell growth and had similar effects on the MCF-7 and MDA-MB-231 spheroids to the free-PTX, suggesting that the liposomal formulation showed promising anti-tumor potentials on breast cancer cells.

Xing et al. [85] investigated the *in vitro* effects of DOX-loaded PEGylated liposomes functionalized with AS1411, a DNA aptamer on MCF-7 cells using flow cytometry and MTT assay. The fluorescence results showed a higher affinity of the DNA aptamer-conjugated DOX liposomes (referred to as Apt-Urn-Lip) towards the MCF-7 cells as opposed to the control liposomes, with a 6.6-fold increase in uptake and drug efficacy. Moreover, the fluorescence response in the MCF-7 incubated for 4 hours

with the treatment was far more evident in the Apt-Urn-Lip than the control liposomes, with 93.6% and 57.0%, respectively.

The cytotoxicity of the Apt-Urn-Lip was further analyzed using the MTT assay. The cells were treated and incubated for 6 hours before further culturing in fresh media for 72 hours. The results indicated that the MCF-7 experienced higher cytotoxicity towards the functionalized liposomes as opposed to the control ones. At a DOX concentration of 500 nM, the cell viabilities were 57.0 ± 6% and 92.4 ± 9%, in the cells treated with Apt-Dox-Lip and control liposomes, respectively. Figure 23 shows confocal microscope images of MCF-7 cells. The nuclei were blue-stained, whereas the DOX was green-labeled; it is apparent that the Apt-Dox-Lip accumulate more and have enhanced uptake by the cells compared to the control liposomes.

A study on HeLa cells was conducted by Bardania et al. [86] where they used the MTT assay to examine the cytotoxicity of RGD-functionalized nanoliposomes (RGD-MNL) encapsulating Eptifibatide. The results showed that the loaded nontargeted nanoliposomes had the most cytotoxic effect on the HeLa cells after incubation for 24 hours at a drug concentration of 200 µg/mL. This suggests that HeLa cells do not overexpress RGD; hence the effect of targeting was not evident.

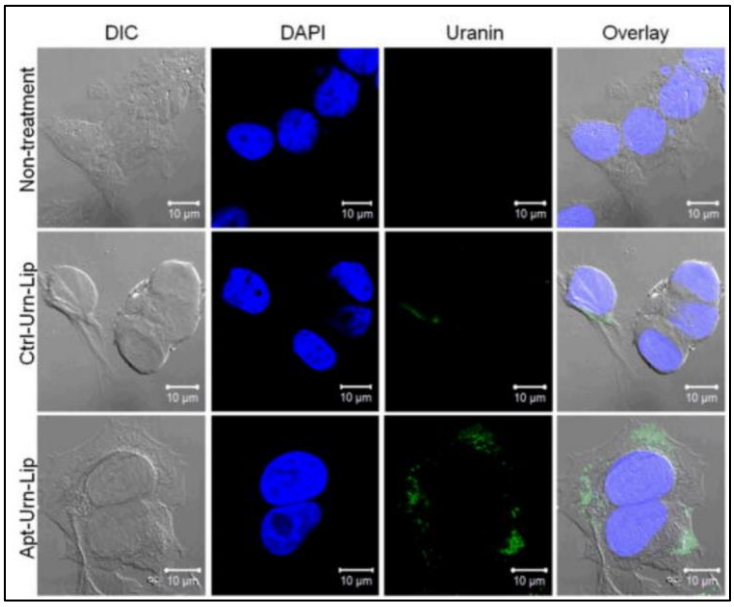

Figure 23: Confocal microscope images of MCF-7 cells treated with Apt-Urn-Lip and Ctrl-Urn-Lip [85]

Chapter 3. Materials and Methods

3.1. Chemical Reagents and Materials

The used chemicals in the preparation of the liposomes include the following: 1,2- dipalmitoyl-sn-glycero-3-phosphocholine (DPPC) and 1,2-distearoyl-sn-glycero-3- phosphoethanolamine-N-[amino(polyethylene glycol)-2000] (DSPE-PEG(200)-NH_2) in powder form were obtained from Avanti Polar Lipids Inc. (Alabaster, AL, USA, supplied by Labco LLC. Dubai, UAE). The cholesterol, HEPES sodium salt, chloroform, Sephadex® G-25, cyanuric acid (2,4,6-Trichloro-1,3,5-triazine), Herceptin powder and Human Serum Albumin (HSA, ≥ 98%) were obtained from Sigma-Aldrich Chemie GmbH (supplied by Labco LLC. Dubai, UAE). Doxorubicin hydrochloride (DOX.HCl) powder was obtained from Euro Asia (Mumbai, India).

3.2. Cell Lines and Culture Conditions

MCF-7, HeLa, SKBR-3, and MDA-MB-231 cell lines were obtained from the European Collection of Authenticated Cell Cultures (ECACC general cell collection, UK). The cells were cultured in Roswell Park Memorial Institute (RPMI-1640) medium and Dulbecco's Modified Eagle Medium (DMEM), supplemented with 10% Fetal Bovine Serum (FBS) and 1% Penicillin/ streptomycin, all were procured from Sigma-Aldrich Chemie GmbH (supplied by Labco LLC. Dubai, UAE). Cells were incubated in a 5% CO_2 incubator at 37 °C for proliferation.

3.3. Synthesis of DSPE-PEG-NH_2 Control Liposomes

The liposome preparation method follows a modified thin-film hydration method found in the literature Figure 24 [87]. In a round bottom flask, the lipids DPPC, DSPE-PEG (2000) amine, and cholesterol are added with respective molar ratios of 13:1:16, and then dissolved using 4 mL of chloroform. The flask is mounted onto a rotary evaporator operating under vacuum at 50 °C and rotating at 90 rpm for 15 minutes, allowing the organic solvent to evaporate slowly, leaving behind a homogenous thin film on the walls.

The dried thin film is then hydrated with a 2-mL Ammonium Sulfate solution to form the liposomal structures and to adjust the pH (about 5.5) to create a pH gradient for DOX encapsulation. The hydrated film is left to rotate without vacuum at 120 rpm and 60 °C for 50 additional minutes. The liposomal suspension is then sonicated for

two minutes in a sonication bath at 60 °C and 40 kHz. Then, extrusion is done using Avanti ® mini-extruder assembly (Avanti Polar Lipids, Inc., Alabaster, AL, USA, supplied by Labco LLC. Dubai, UAE), where the liposomes are passed 30 times through a 0.2-µm polycarbonate membrane.

To purify the liposomes from any excess unencapsulated material, size exclusion chromatography gel filtration is carried out. To prepare the column, 1.5 g of G-25 is dissolved in 10 mL phosphate buffered saline (PBS) and left to hydrate for 2 hours ahead of use. The collected liposome fractions are kept stored in Eppendorf tubes at 4 °C until used.

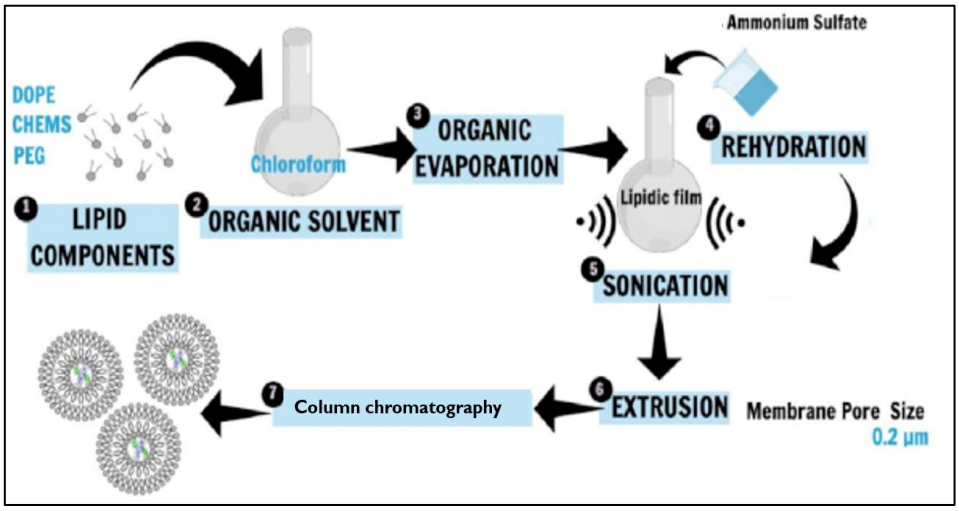

Figure 24: Illustrative schematic of the thin film hydration synthesis method [87]

3.4. Loading of DOX into DSPE-PEG2000-NH_2 Liposomes

To load the drug into the liposomes, a modified pH gradient method [88] was adopted. Ammonium Sulfate is preferred for creating the pH gradient as it yields high encapsulation amounts of DOX into the liposomes. The DSPE-PEG2000-NH_2 liposomes (control liposomes) are passed through a single column of 1.5 g of G-25 and equilibrated with 10 mL HBS prepared at least 2 hours ahead of time. This step is mandatory in order to alter the extravesicular pH of the liposomes to 7.4, while the intraliposomal pH is acidic; thus, a driving pH gradient is maintained to facilitate the loading of DOX.

The liposomal solution is then collected in a glass vial where a 1:25 (w/w) drug:lipid ratio is attained by adding 250 µL of DOX (16 mg DOX powder per mL

HBS stock solution) and leaving it to stir at 60 °C and 80 rpm for 40 minutes. Then, the loaded liposomes are passed through another single gel-filtration column, which is equilibrated with 1.5 g G-25 dissolved in 10 mL borate buffered saline (BBS) in order to get rid of excess DOX and prepare the liposomes for conjugation.

3.5. Synthesis of Human Serum Albumin Conjugated Liposomes

The BBS slightly alkalizes the liposomal formulation pH to about 8.5 in order to prepare for the double-displacement conjugation reaction. The PEG terminus of the liposomes is activated using cyanuric chloride (CC) as a coupling agent for the protein to bind Figure 25 [39]. A CC solution is prepared by dissolving 10 mg of CC powder in 1 mL pure acetone and 0.5 mL distilled water, from which 28 µL is added to the loaded liposomes. The reaction takes place in an ice bath at 0 °C for 3 hours with gentle stirring. After 3 hours, 75 µL of HSA solution (10 mg HSA powder dissolved in 1 mL BBS stock solution) is added to the vial, and the reaction is left overnight. To collect the loaded-targeted liposomes (HSA-DOX liposomes), the sample is centrifuged for an hour at 4 °C and 18000 rpm. The very low temperature is to ensure the elimination of any heating effects on the liposomes due to centrifugation at high speed for a considerable duration. The liposomal pellet is collected and resuspended according to use.

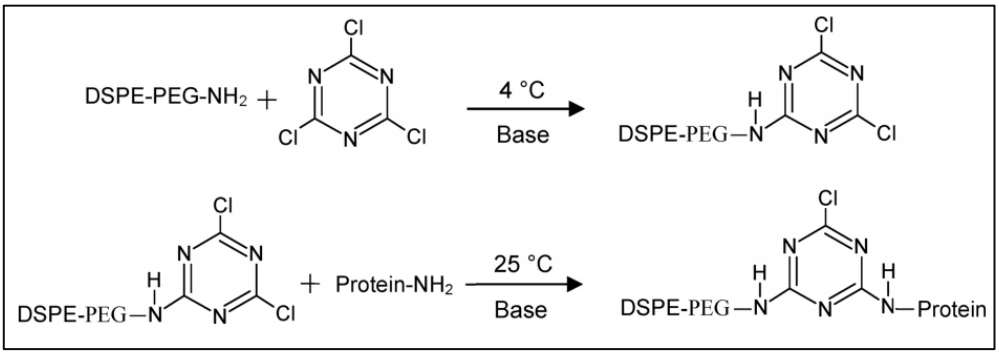

Figure 25: The protein conjugation reaction using cyanuricc chloride as a coupling agent [39]

3.6. Synthesis of Herceptin Conjugated Liposomes

For the conjugation of Herceptin to the DSPE-PEG2000-NH_2 liposomes, a similar protocol is followed. A CC solution is prepared by dissolving 10 mg CC powder in 1 mL pure acetone. In a separate vial, 0.5 mL of deionized water is added, to which 9.23 µL of the CC solution is added. To the final solution in the vial, 1 mL of the loaded

liposomes is added and is left to stir in an ice bath at 80 rpm for 3 hours. Then, 1 mg Herceptin is dissolved in 0.5 mL BBS and is added to the reaction vial, and is left to stir overnight in the bath, gently. Centrifuging is used to collect the loaded-conjugated liposomes (HER-DOX liposomes), as mentioned above.

3.7. Procedure for the MTT Assay

The MTT assay protocol was adapted from the literature [75] and slightly modified for the purposes of this research Figure 26. The same procedure was followed for all cell lines. MCF-7 and MDA-MB-231 cells were cultured in RPMI-1640, whereas HeLa and SKBR-3 cells were cultured in DMEM. Aliquots containing $1x10^4$ cells per well were seeded into 96-well plates and incubated for 24 hours prior to treatment to ensure proper cellular confluency. After 24 hours, different treatments were added in triplicates to the cells with a concentration of 8 µM per well.

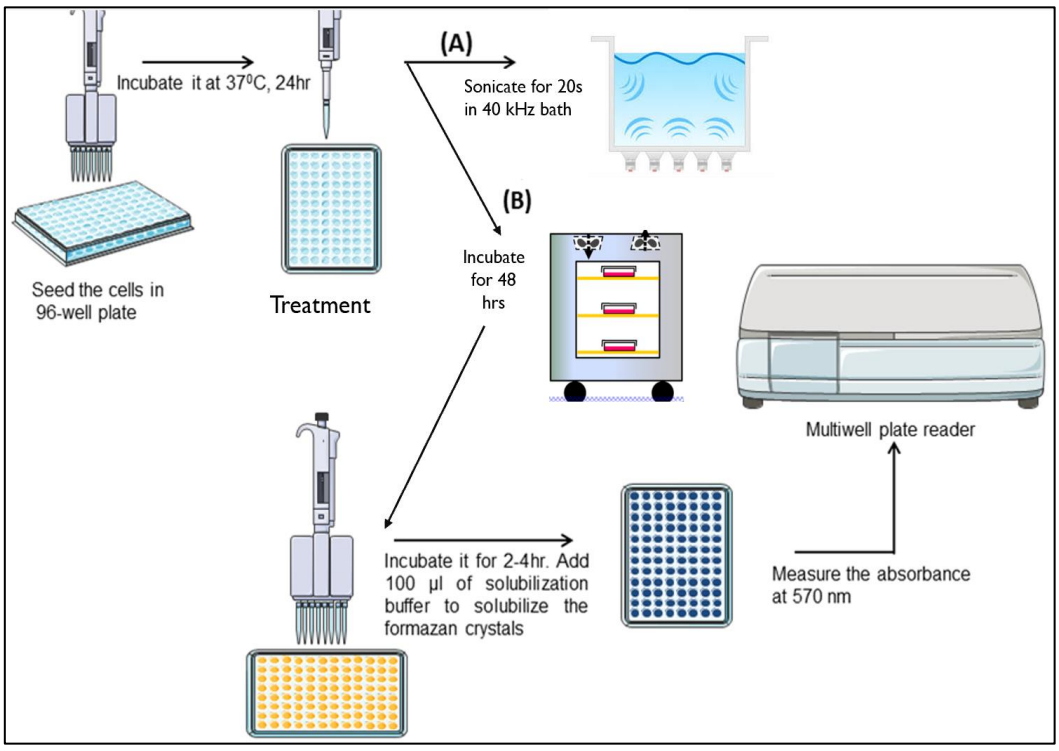

Figure 26: Schematic illustrating the followed MTT assay protocol

The different treatment groups included free DOX prepared by dissolving 2.9 mg DOX powder in 5 mL DMSO, DOX- DSPE-PEG2000-NH2 (Control) liposomes, and the two types of conjugated liposomes, accordingly. For every independent experiment, two plates of each cell line were treated. The plates were then incubated

for 5 hours before exposing one of them to US for 20 seconds in a 40 kHz sonication bath. After 48 hours of post-treatment incubation, the old media was replaced with fresh media mixed with a 10% (v/v) MTT solution.

After 2-4 hours of incubation, the old media was discarded, and 100 µL of DMSO was added per well to ensure the complete dissolution of the purple formazan crystals. The plates were left for 10 minutes before taking the absorbance readings in the ELISA M965+ microplate spectrophotometer (Metertech, India). The detailed protocol adopted for one independent cell work experiment is as follows, i.e., for one cell line and one liposomal treatment:

1. The seeding process starts by discarding the old medium from the T-75 flask and then washing it with Dulbecco's phosphate-buffered saline (DPBS) to remove any traces of the medium, preparing for trypsinization. Once the DPBS is discarded, 2 ml of trypsin, a digestive enzyme that detaches the cells from the flask, is added and the flask is incubated for 3 minutes. Then, 2 ml of medium is added to the trypsinized flask, which by now should have the cells floating, to stop the action of trypsin. The 4 ml solution is centrifuged for 2 minutes at 2000 rpm to collect the cellular pellet at the bottom, where the pink layer is decanted, and 2 ml of media is added to resuspend the cells.

2. A cell count is carried out on the stock solution to determine the necessary dilution, in order to achieve a final concentration of $1x10^4$ cells/per well. So, 50 µL of the stock solution is carefully mixed with 50 µL trypan blue, and a small amount is pipetted to the chip disposable hemocytometer, which is then mounted into the automated cell counter Figure 27 [89]. After adding the adequate amount of medium to the cell stock to achieve the desired concentration, cells are seeded with an approximate density of $1x10^6$ cells/plate. Two plates are prepared.

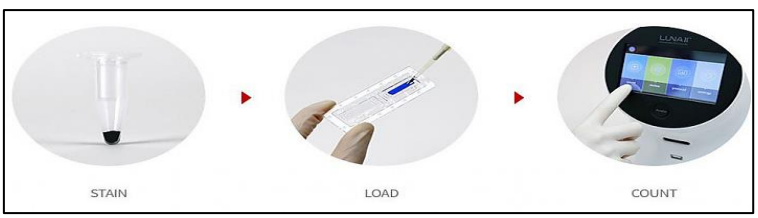

Figure 27: The process of automated cell counting [89]

3. After a 24-hours incubation period to ensure the cells confluency, both plates receive the exact treatments in triplicates. Three wells are left for control, three are treated with free DOX, three are treated with the conjugated-liposomal DOX, and three are treated with liposomal DOX. After adding the treatments, the plates are incubated for a period of 5 hours to allow the different formulations to act on the cells. Five hours post-treatment incubation, one of the plates is sonicated in a 40-kHz bath for 20 seconds and then incubated again to allow any of the alive detached cells, due to US exposure, to settle down. After an hour, the media of both plates is replaced, and the plates are incubated for 48 hours.

4. On the fourth day of the experiment, the MTT reagent is added with a quantity of 10% of the well volume to all plates. The plates are then incubated for at least two hours, to allow the reduction reaction to take place. Once the purple formazan crystals form, the old media is discarded, and 100 μL of DMSO is added to dissolve the crystals. The plates should be kept in a dark place for 10 minutes, and then the readings can be taken.

3.8. Characterization of Liposomes

3.8.1. Determination of liposomes size by dynamic light scattering. The size distribution of the liposomal drug can significantly alter its characteristics and performance in the biological system. Many important characteristics such as the encapsulation capacity, aggregation tendency, sedimentation behavior, drug biodistribution, circulation time and elimination by the MPS are considerably size-dependent.

Therefore, the technique of dynamic light scattering (DLS) was employed to determine the liposomes hydrodynamic radius, polydispersity, and size distribution. It is one of the most suitable methods because it provides very accurate measurements of particles' sizes in the sub-micron range [90].

The underlying principle by which this technique works is based on the concept of Brownian motion. It postulates that the movement of suspended particles in a given medium is random, due to the rapid continuous collisions between the suspended particles and the moving molecules of the suspending fluid.

The DLS machine has a laser of a pre-determined wavelength in it. Once the laser is focused on the sample, a detector collects and detects the scattered light's intensity due to the particles' random movement. Afterward, a specific algorithm-based process is employed to analyze the instrumental data, which is in the form of time-dependent fluctuations in the scattered light intensity, to a meaningful particle size distribution [91].

The samples were prepared by diluting 15 µL of the liposomes in 1 mL PBS then loading them into a cuvette and into the DynaPro® NanoStar™ (Wyatt Technology Corp., CA, USA) DLS machine. The criteria for acceptable batches of liposomes are to have a mean size ranging from 80 to 150 nm and a % polydispersity <20%, indicating monodispersed unilamellar liposomes.

3.8.2. Estimation of phospholipid content using Stewart assay. To quantify the phospholipid content of the liposomes, a calorimetric approach is used. The Stewart assay is based on the ability of phospholipids to form a complex with ammonium ferrothiocyanate (FTC). The complex is soluble in chloroform, whereas FTC, which is a dark red inorganic compound, is not. Thus, when FTC is added to a liposomal-chloroform mixture, a biphasic system of two immiscible layers forms [92].

The protocol for one independent experiment is as follows: to break up the liposomes and dry up the suspension medium, 50 µL of the liposomes is added to a 50 ml round bottom flask and mounted into the rotary evaporator under vacuum at 45 °C for 15 minutes.

Then, 1 ml of chloroform is added to the flask to resuspend the liposomes, and the mixture is sonicated for 10 minutes in a 40-kHz bath to make sure that all DPPC is dissolved in the chloroform. The samples are then prepared by adding varying amounts of the liposomes, with chloroform and FTC as detailed in Table 1.

Samples 1, 1A, 2, 2A, 3, and 3A are control liposomes, whereas samples 4, 4A, 5, 5A, 6 and 6A are the targeted liposomes. Duplicates are made (annotated with A) for each sample to ensure the accuracy of measurement and eliminate the chances of human errors. The samples are then vortexed for 30 seconds to provide contact time for FTC to react with the dissolved DPPC in the chloroform. Afterward, the samples are centrifuged for 10 minutes at 1000 rpm to separate the two immiscible phases.

Next, a Pasteur pipette is used to extract the bottom transparent layer, which contains the dissolved complex of interest, and is loaded into a quartz cuvette, and the top layer, which contains the deep red inorganic reagent, is discarded into an inorganic waste container. The samples' absorbance is measured at 485 nm against the blank baseline, using the Evolution^{TM} 60S Ultraviolet-visible (UV-VIS) spectrophotometer (Thermo Fisher Scientific, Waltham, MA, USA). Finally, the amount of DPPC in the samples can be obtained using a calibration curve.

Table 1: Stewart assay samples preparation

Centrifuge tube #		**Liposomes(µL)**	**Chloroform(µL)**	**FTC(µL)**
1	**1A**	75	1925	2000
2	**2A**	125	1875	2000
3	**3A**	200	1800	2000
4	**4A**	75	1925	2000
5	**5A**	125	1875	2000
6	**6A**	200	1800	2000
Blank		0	2000	2000

3.8.3. Protein quantitation using bicinchoninic acid (BCA) assay. The bicinchoninic acid (BCA) assay is a colorimetric assay used to quantify the protein content of the synthesized liposomes. It is used to confirm that conjugation has occurred and that the composition of the functionalized liposomes is different than the control ones. It was first introduced in 1985 [93], and it has become prevalent due to its practicality, accuracy, and high sensitivity.

There are two main subsequent reactions that take place, as illustrated in Figure 28. The first reaction is called the biuret reaction, where the cupric ions are reduced, by peptide bonds in proteins, to cuprous ions under alkaline conditions. The amount of copper reduced depends on the protein concentration in the sample.

Then, it follows that each cuprous ion is chelated by two reagent molecules to form a purple complex [93]. The formed purple complex has a peak absorbance at 562 nm that can be measured using the Ultraviolet-visible (UV-VIS) spectrophotometer

[94]. The same procedure was done for both types of liposomes, HSA-DOX, and HER-DOX liposomes.

The following amounts are for one independent experiment, which needs 400 µL of each type of liposomes and 7 ml of the working reagent, prepared in the fixed ratio of 25:25:1. To begin, the working reagent is prepared by mixing 3.5 ml of QuantiPro TM buffer QA with 3.5 mL of QuantiPro TM buffer QB and 140 µL of the $CuSO_4$ solution (Sigma Aldrich Chemie GmbH (supplied through LABCO LLC. Dubai, UAE). It will form a light green solution.

Then, 7 samples are prepared as detailed in Table 2, where 1 sample is the blank reference consisting of PBS and the working reagent, 3 samples of control liposomes added to PBS and the working reagent, and 3 other samples of the conjugated liposomes added to PBS and the working reagent as well.

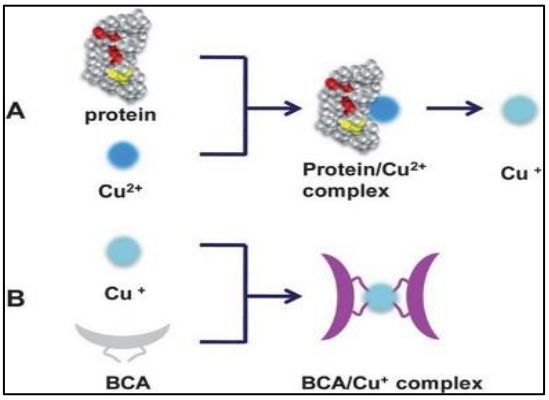

Figure 28: Schematic illustrating the two-steps reaction involved in the BCA assay [91]

Table 2: BCA assay samples preparation

Sample #	Liposomes(µL)	PBS(µL)	BCA reagent(µL)
Blank	-	1000	1000
Control Lip. 1	200	800	1000
Control Lip. 2	100	900	1000
Control Lip. 3	100	900	1000
Conjugated Lip. 1	200	800	1000
Conjugated Lip. 2	100	900	1000
Conjugated Lip. 3	100	900	1000

After the samples are loaded into Eppendorf tubes, they are incubated for an hour in a 60 ºC bath, and then left for about 15 minutes to cool to room temperature. If some of the samples appear to be turbid, they can be centrifuged for 20 minutes at about 18000 rpm to settle down the suspended proteins. Afterwards, they are transferred to cuvettes, and the absorbance is measured against the blank at 562 nm in the Evolution™ 60S Ultraviolet-visible (UV-VIS) spectrophotometer (Thermo Fisher Scientific, Waltham, MA, USA).

3.9. Statistical Analysis

To evaluate the significance of the quantitative data generated in this research, comparative statistical analysis was carried out to compare the differences between experimental groups' mean values. The chosen hypothesis-testing test is the two-tailed independent samples t-test, also known as the two-sample t-test and student's t-test. It is used to determine if the difference between two means of two groups is randomly obtained by chance, or it actually follows from manipulating the experimental variables [95].

Also, it can be translated to a comparative indicator depending on the context; for instance, it could be used to imply if a new treatment is superior to another already existing one. So, this is the most appropriate comparative test choice, since this research is based on an independent categorical variable that has two groups (treatments in the presence and absence of US), and one continuous dependent variable (i.e., cell viability in response to the different treatments).

The two-sample t-test has a number of assumptions that the underlying distributions must follow, including that the means of the samples must be independent of each other, the data must be continuous, and the variances of the samples are equal [96]. To test the assumption of homoscedasticity or homogeneity of variances, the Levene test was also carried out. Levene's test null hypothesis is: $H_o = \sigma 2_1 = \sigma 2_2 = \cdots = \sigma 2_k$. A significance level of 0.05 (p-value < 5%) is set as a cut point to either accept or reject the hypothesis.

Thus, if the Levene's significant value is greater than 0.05, the null hypothesis is accepted, and it is proved that the data sets fulfill the homogeneity of variance assumption [96]. It is necessary to ensure that the variances are equal because the t-test

is not considered robust in the case of unequal variances, as it can lead to inaccurate conclusions.

Another measurement that was computed for the different data sets, to check for their internal consistency and reliability, is Chronbach's coefficient alpha (α). It was developed by Lee Cronbach in 1951 [95]. Its value ranges between 0 and 1; where the closer the value is to unity, the greater is the internal consistency of the readings. It is not considered a statistical test, but it is rather an estimator of how closely related are the readings in a data set. Consequently, the outcomes of the independent samples t-test can help in either rejecting or accepting the experiments' null hypothesis.

The null hypothesis assumes that the means of the two groups are equal, meaning that the experimental manipulation has no effect, but the changes were rather due to chance [96]. In this study, the hypotheses are formulated as follows:

- 1^{st} null hypothesis: US exposure has insignificant effects on the performance, cellular uptake, and cytotoxicity of neither the control nor the conjugated liposomes on both positive and negative cell lines.
- 2^{nd} null hypothesis: for the positive cell lines which overexpress the moiety's receptors on their surface, the cellular uptake and cytotoxicity of the control liposomes are similar to the conjugated ones, whether in the absence or presence of US.
- 3^{rd} null hypothesis: for the negative cell lines which do not overexpress the moiety's receptors on their surface, the cellular uptake and cytotoxicity of the control liposomes are similar to the conjugated ones, whether in the absence or presence of US.

In this work, Microsoft Excel® was used to construct the heat maps which summarize the p-values for the different tested combinations, and the IBM® SPSS® statistics software was used to compute the Levene's test significance and Chronback's alpha coefficient values.

Chapter 4. Results and Discussion

4.1. Estimation of Liposome Size Using Dynamic Light Scattering (DLS)

The hydrodynamic radii and polydispersity indices (% Pd) of three batches of each liposome type were measured using DLS. The measurements were then averaged, as shown in Table 3. The mean sizes are reported as means ± standard deviation:

- Control liposomes size is 83.5 ± 0.734 nm and a pd% of 14.3 ± 1.15
- Albumin liposomes size is 101 ± 1.56 nm and a pd% of 13.9 ± 1.41
- Herceptin liposomes size is 103 ± 1.86 nm and a pd% of 16.5 ± 1.88

Table 3: Summary of DLS results for three types of liposomes

	Control Lip.		**HSA-DOX Lip.**		**HER-DOX Lip.**	
	Radius (nm)	% Pd	Radius (nm)	% Pd	Radius (nm)	% Pd
Run 1	83.6	9.94	98.5	14.1	103	16.4
Run 2	83.6	18.0	102	14.3	101	14.6
Run 3	83.4	15.2	103	13.5	104	19.2
Average	**83.5**	**14.4**	**101**	**13.9**	**103**	**16.5**

There is a significant difference in size between control and HSA-DOX liposomes (p-value = 0.005) as well as between the control and HER-DOX liposomes (p-value = $2x10^{-3}$). The HER-DOX liposomes are slightly larger than the HSA-DOX nanoparticles, which could be attributed to the molecular weight of Herceptin (148 kDa) [51], which is almost 2.2 folds more than that of HSA (66.5 kDa) [46]. Therefore, it is confirmed that the liposomes are large unilamellar vesicles, and they can benefit from the enhanced permeability and retention (EPR) effect. Lastly, the liposomes produced in this work are very similar in morphology, size, and structure to those presented in Awad et al. [39] work, shown in Figure 29.

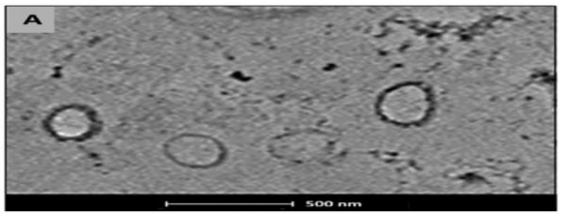

Figure 29: Transmission electron microscopy (TEM) image of calcein-loaded transferrin-conjugated liposomes (500 nm scale) [39]

4.2. Estimation of Lipid Concentration Using Stewart's Assay

To measure the amount of lipids in each type of liposomes, a calibration curve relating the lipid content to the absorbance readings was prepared Figure 30. Using the least-squares regression analysis, the equation of the line yielded a high correlation coefficient (R^2= 0.9918), thus confirming the linearity of the calibration curve.

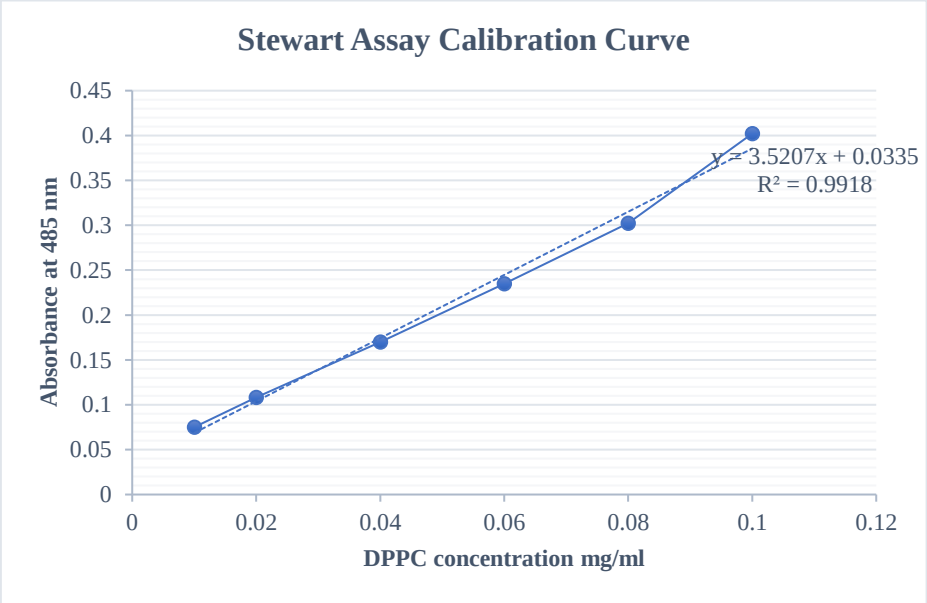

Figure 30: Stewart assay calibration curve

Three independent experiments were carried out for each type of liposomes: control liposomes, HSA-DOX liposomes, and HER-DOX liposomes. The control liposomes had a lipid content of 16.9 mg/ml, whereas the HSA-DOX liposomes had a lipid content of 7.47 mg/ml (p-value=$1.7x10^{-2}$). The lipid content in the control liposomes is almost twice that in HSA-DOX liposomes, which could be due to the HSA conjugation reaction and the final purification steps in the synthesis.

HSA-DOX liposomes were purified by passing them through a double-stage gel filtration column, whereas the control liposomes were purified by passing them through a single Sephadex G-25 column. On the other hand, HER-DOX liposomes and control liposomes were found to have similar lipid contents of 13.5 mg/ml and 15.3 mg/ml, respectively, indicating insignificant differences (p-value=$6.2x10^{-1}$).

4.3. Estimation of Protein Concentration Using BCA Assay

In order to quantify the protein content of the different liposomal formulations, a calibration curve for the BCA was produced Figure 31. The increase in protein content

in the moiety-bound liposomes confirms that the conjugation reactions successfully took place.

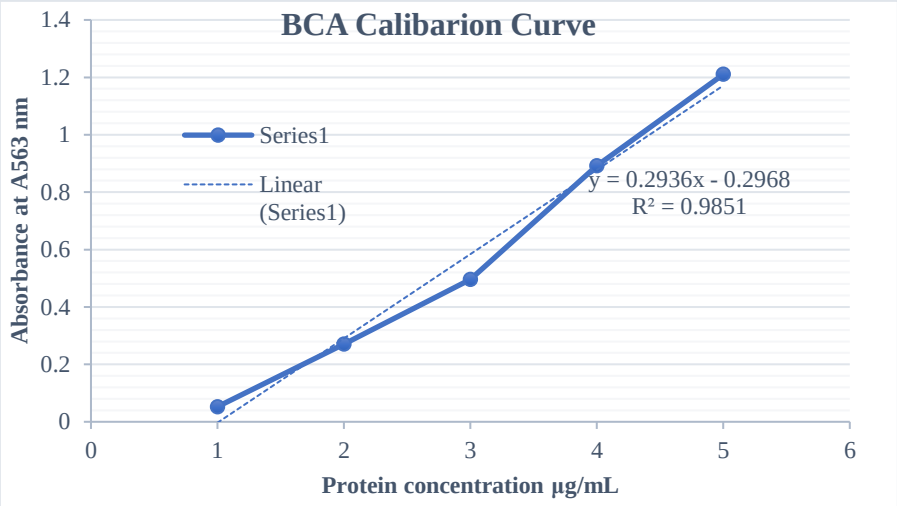

Figure 31: BCA calibration curve.

Table 4 summarizes the results for the different types of liposomes. HSA-DOX and control liposomes have a protein content of 0.068 µg/mL and 0.012 µg/mL (p-value=$4x10^{-3}$), respectively, indicating that the conjugated liposomes have 5.5-fold higher protein. The HER-DOX liposomes were found to have a protein content of 0.024 µg/mL, and their controls had a protein content of 0.016 µg/mL (p-value=$1x10^{-2}$), indicating that the HER-DOX liposomes have a 1.5-fold higher protein concentration. The higher protein content in HSA-DOX liposomes compared to HER-DOX liposomes could be due to the size of the proteins, the HSA molecule is smaller in size (66.5 kDa) compared to Herceptin (148 kDa), thus more could bind to the liposomes' surface.

Table 4: Summary of BCA results for three types of liposomes.

	Control liposomes	**HSA-DOX liposomes**	**Control liposomes**	**HER-DOX liposomes**
Run 1	0.012348	0.066455	0.011589	0.019281
Run 2	0.01288	0.075675	0.015672	0.024513
Run 3	0.011522	0.061945	0.021332	0.02753
Average Protein content (µg/ml)	**0.01225**	**0.06802**	**0.01619**	**0.02377**

4.3. MTT Assays Results

This section displays the MTT results (mean ± SD %, n=3) of three independent experiments associated with the HSA-DOX liposomes in MCF-7 and HeLa cell lines and HER-DOX liposomes in SKBR-3 and MDA-MB-231 cell lines. A comparison of the performance of free DOX across both cell lines, with and without exposure to US, suggested that US exposure has a visible effect on the action and uptake of free DOX.

For instance, the cell viability percentage of MCF-7 cells treated with free DOX, in the presence of US was 7.9%, while it was 11.7% in the absence of US exposure (p-value= 1.68×10^{-4}). This observation is in agreement with literature [73], which proves that the US, on its own, promotes the penetration of the drug through cellular membranes by inducing pores.

A similar trend is also observed when comparing the performance of the liposomal formulations, in the presence and absence of US, in both cell lines. So, whether the drug is sequestered and loaded into a nanocarrier or it is freely administered, sonoporation significantly enhances its uptake by the cells. The p-values obtained from the experiments using the MCF-7 cell line are summarized in the heat map Table 5, which indicates that US exposure has significant effects on the cells uptake of the different treatments.

Figure 32 shows the MCF-7 cells viability % in response to the different treatments. Cells treated with HSA-DOX paired with US showed more pronounced effects than in the absence of US, as the exhibited cell viabilities were 15.1 ± 0.613% and 60.9 ± 3.87% (p-value=7.78×10^{-5}), respectively. As for the control liposomes, cells exhibited 39.4 ± 0.499% and 71.6± 1.39% cell viabilities (p-value=6.59×10^{-6}), with and without US exposure, respectively. The results suggest that US exposure significantly enhanced the cellular uptake of both the targeted and control liposomes, thus highlighting the synergistic effects of combining US with the liposomal drug delivery system.

In terms of liposomal superiority in both US exposed and unexposed groups, HSA-DOX treated cells exhibited a smaller percentage of viable cells than its natural counterpart, suggesting that active targeting enhances drug uptake by receptor-mediated endocytosis.

Table 5: Heat map summarizing p-values for the MCF-7 cell line

	Untreated	Untreated +US	DOX	DOX+ US	CONTROL	CONTROL +US	ALB-DOX	ALB-DOX+ US
Untreated	1	8.92E-01	4.53E-10	4.13E-12	8.44E-06	6.90E-09	1.40 E-04	4.08E-09
Untreated +US	8.92E-01	1	4.53E-10	4.13E-12	8.44E-06	6.90E-09	1.40 E-04	4.08E-09
DOX	4.53E-10	4.53E-10	1	1.68E-04	4.95E-07	3.75E-07	5.68 E-05	2.53E-03
DOX+US	4.13E-12	4.13E-12	1.68E-04	1	3.44E-07	1.06E-07	4.19 E-05	8.59E-05
CONTROL	8.44E-06	8.44E-06	4.95E-07	3.44E-07	1	6.59E-06	2.17 E-02	7.79E-07
CONTROL +US	6.90E-09	6.90E-09	3.75E-07	1.06E-07	6.59E-06	1	1.45 E-03	1.67E-06
ALB-DOX	1.40E-04	1.40E-04	5.68E-05	4.19E-05	2.17E-02	1.45E-03	1	7.78E-05
ALB-DOX+US	4.08E-09	4.08E-09	2.53E-03	8.59E-05	7.79E-07	1.67E-06	7.78 E-05	1

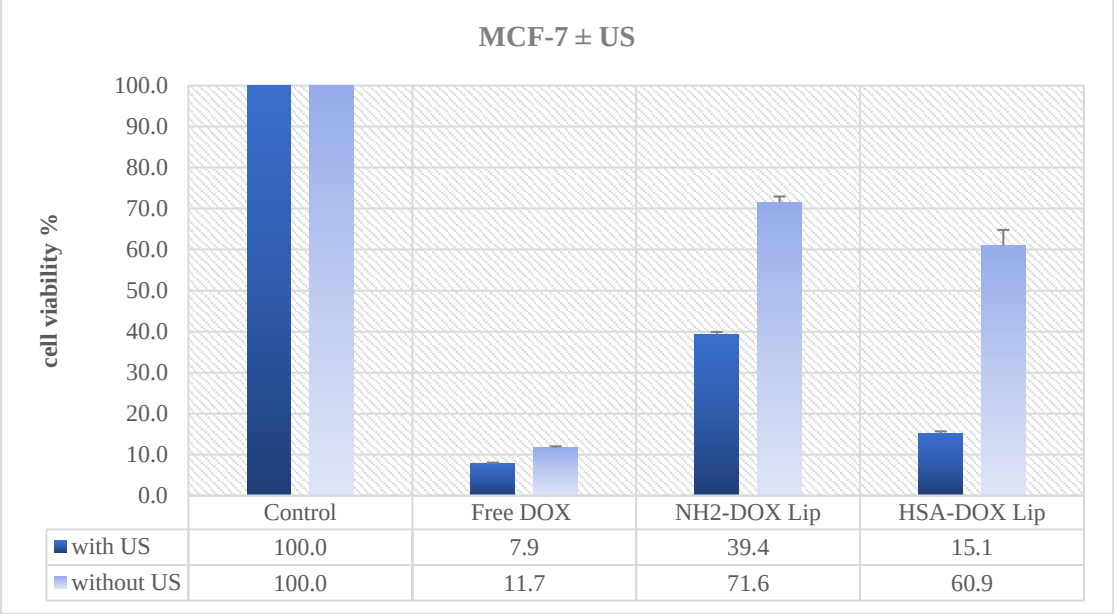

Figure 32: MCF-7 cells cell viability % in response to the different treatment groups. Data are representative of three independent experiments.

The results are aligned with those reported in the literature as supported by a previously discussed study [83], which showed increased cellular uptake of PEGylated HSA liposomes by MCF-7 cells upon exposure to US. Jiang et al. [97]investigated the effect of conjugating nanoparticles with different concentrations of Albumin on the cellular uptake of several cell lines. In Figure 33, the red line shows the enhanced uptake of the nanoparticles by the MCF-7 cells as the % of albumin content increases. This conclusion further supports the claim that albumin targeted nanocarriers have a higher

affinity towards MCF-7 cells, because more of the anti-neoplastic agent was internalized by the cells as a result of active targeting.

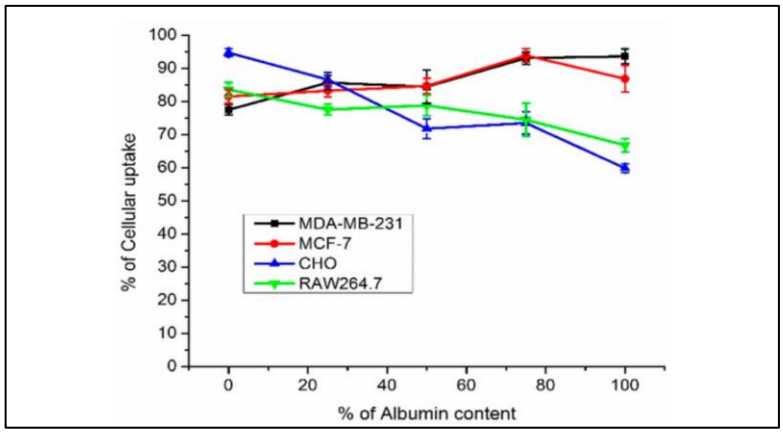

Figure 33: Different cell lines uptake of the nanoparticles with respect to % of albumin content [97]

In order to validate the comparison and emphasize the effects of both US exposure and active targeting by functionalizing with a moiety, the same set of experiments was carried out on human cervical cancer HeLa cell line, which does not overexpress HSA. Figure 34 shows the cell viability percentages in response to different treatments.

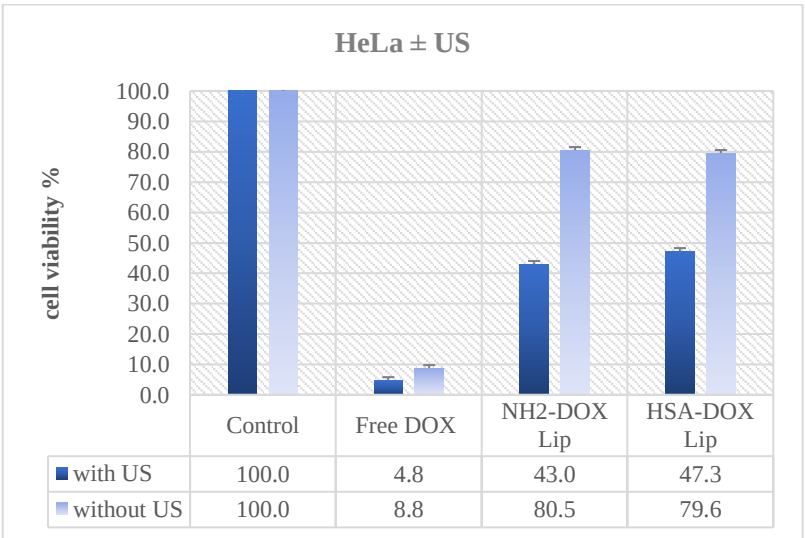

Figure 34: HeLa cells cell viability % in response to the different treatment groups. Data are representative of three independent experiments

HeLa cells treated with control liposomes and HSA-DOX liposomes coupled with US exposure exhibited cell viabilities of 43.0 ± 4.30 % and 47.3 ± 0.621 % (p-

value = $2.37x10^{-1}$), whereas without US exposure, the percentages were higher with cell viabilities of 80.5 ± 0.449% and 79.6 ± 0.262 % (p-value = $5.70x10^{-2}$), respectively. Thus, both liposomal formulations show similar effects on cell viability within groups of US exposure and absence. These results are expected since HeLa is an HSA-negative cell line, so functionalization of the liposomes did not significantly alter liposomes accumulation and internalization by the cells. Moreover, a similar conclusion is grasped that US and liposomes seem to work synergistically to aid in DOX uptake, as cells treated with liposomal DOX in the absence of US exhibited higher cell viability. As observed, the control liposomes with US exposure exhibited the best combination. The p-value results are summarized in the heat map Table 6.

Table 6: Heat map summarizing p-values for the HeLa cell line.

	Untreated	**Untreated +US**	**DOX**	**DOX+ US**	**CONTROL**	**CONTROL +US**	**ALB-DOX**	**ALB-DOX+ US**
Untreated	1	7.53E-1	2.35E-11	5.12E-11	4.25E-07	4.77E-05	4.08E-08	2.90E-08
Untreated +US	7.53E-01	1	2.35E-11	5.12E-11	4.25E-07	4.77E-05	4.08E-08	2.90E-08
DOX	2.35E-11	2.35E-11	1	4.38E-05	3.12E-09	3.54E-04	6.20E-10	1.19E-07
DOX+US	5.12E-11	5.12E-11	4.38E-05	1	2.96E-09	2.31E-04	7.13E-10	8.86E-08
CONTROL	4.25E-07	4.25E-07	3.12E-09	2.96E-09	1	2.53E-04	5.72E-02	4.24E-07
CONTROL +US	4.77E-05	4.77E-05	3.54E-04	2.31E-04	2.53E-04	1	2.77E-04	2.37E-01
ALB-DOX	4.08E-08	4.08E-08	6.20E-10	7.13E-10	5.72E-02	2.77E-04	1	2.86E-07
ALB-DOX+US	2.90E-08	2.90E-08	1.19E-07	8.86E-08	4.24E-07	2.37E-01	2.86E-07	1

A final comparison of the response of both cell lines to the liposomal treatments with and without US exposure is illustrated in Figure 35. US exposure did indeed enhance cellular uptake of liposomal DOX, as cell viabilities are considerably lower in the treatments exposed to US.

Moreover, the action of HSA functionalized liposomes with US exposure showed far higher drug efficacy in MCF-7 cells than in HeLa cells, as the exhibited cell viabilities were 15.7 ± 0.613 % and 47.3 ± 0.621% (p-value=$8.05x10^{-7}$), respectively.

However, the action of the control liposomes in the presence of US did not differ between both cell lines (p-value=$2.99x10^{-1}$), signifying the effects of active-targeting. Therefore, active targeting combined with US exposure yields the most

promising results and enhances receptor-mediated endocytosis in the receptor-overexpressing cell line.

Similar observations and conclusions can be drawn from analyzing the MTT results collected to investigate the performance of Herceptin-conjugated liposomes. Three independent experiments (mean ± SD %, n=3) were carried out on SKBR-3 cells and MDA-MB-231 cells, HER2-positive and negative cell lines.

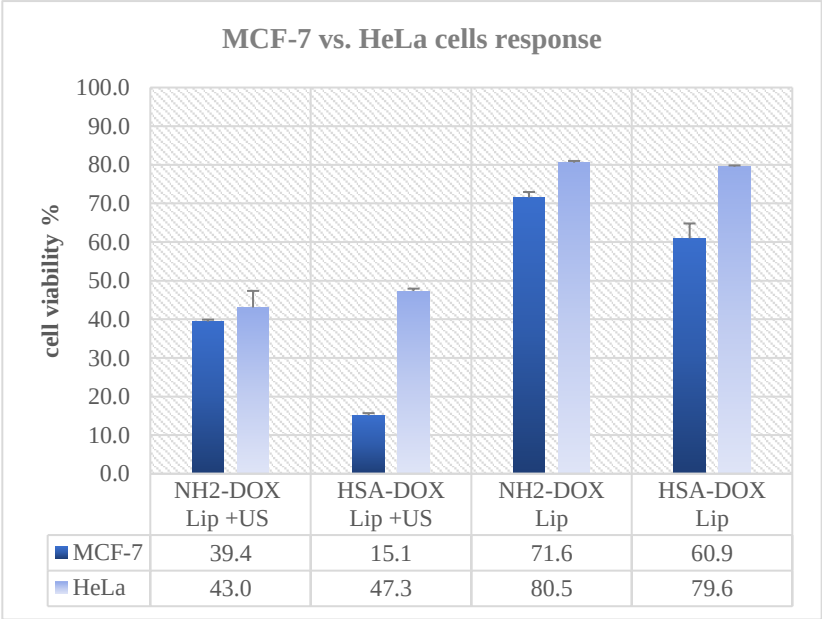

Figure 35: comparison of the cell viability % of the MCF-7 vs. HeLa cell lines

Moving on, Figure 36 summarizes the cell viability percentages of SKBR-3 in response to different treatments. Comparing the viabilities under the exposure and absence of US, there are significant differences, whether it is the free drug or the liposomal formulations, as observed in the heat map Table 7. Thus, US has predominant effects in enhancing the drug's uptake due to sonoporation, as already discussed.

Particularly, it is noteworthy to mention that the effects of active-targeting are enhanced in the presence of US, as observed when comparing the viabilities of cells treated with control liposomes and those treated with HER-functionalized liposomes, 32.9 ± 1.31 % and 27.4 ± 0.260 %, respectively (p-value=4.58×10^{-3}).

Following the same approach to validate the comparison and emphasize the effects of both US exposure and active-targeting, the same set of experiments was

carried out on a HER2- negative cell line, i.e., MDA-MB-231. Figure 37 shows the cell viability percentages in response to the different treatments.

The performance of both control and HER-functionalized liposomes was similar, with US exposure or without. That is, the cell viability percentage in the presence of US of cells treated with control liposomes and HER liposomes is 38.7 ± 0.858 % and 40.1 ± 0.216 %, respectively (p-value=$9.4x10^{-2}$).

This observation is expected since MDA-MB-231 cells do not overexpress HER2 receptors on their surface. However, when comparing the performance of the free drug and either liposomal formulations in the presence and absence of US, it is noticeable that US enhances the uptake of the treatment Table 8.

A final comparison of the response of both cell lines to the liposomal treatments with and without US exposure is illustrated in Figure 38. US exposure did indeed enhance cellular uptake of liposomal DOX, as cell viabilities are considerably lower in the US exposed groups. Moreover, the action of HER functionalized liposomes with US exposure showed far higher drug efficacy in SKBR-3 cells than in MDA-MB-231 cells, as the exhibited cell viabilities were 27.4 ± 0.260 % and 40.1 ± 0.216% (p-value=$7.53x10^{-7}$), respectively.

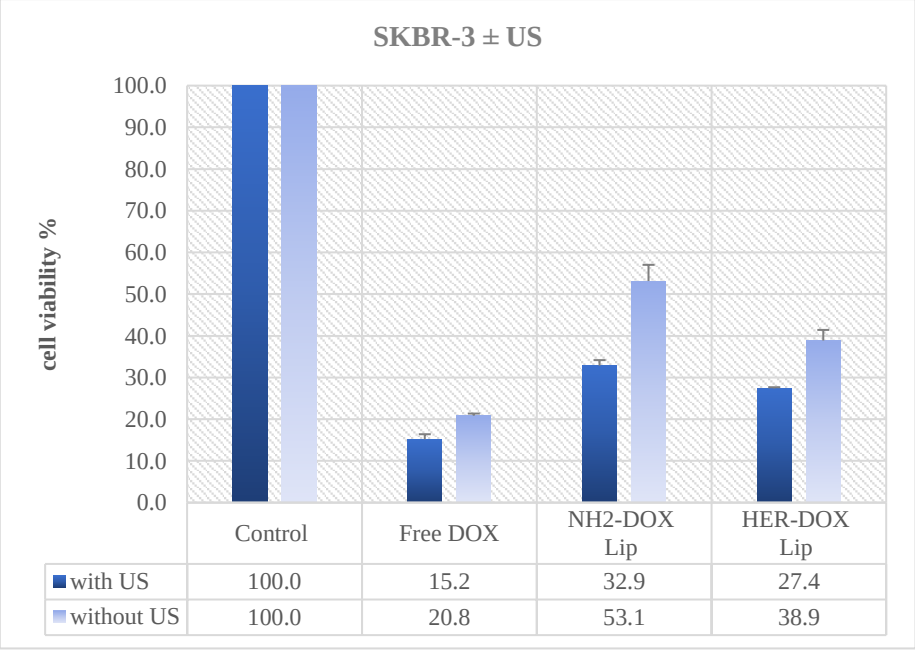

Figure 36: SKBR-3 cell viability % in response to the different treatment groups Data are representative of three independent experiments.

Table 7: Heat map summarizing p-values for the SKBR-3 cell line.

	Untreated	**Untreated +US**	**DOX**	**DOX+ US**	**CONTROL**	**CONTROL +US**	**HER-DOX**	**HER-DOX+ US**
Untreated	1	5.80E-01	2.90E-09	6.51E-08	6.98E-05	2.20E-07	4.48E-06	2.46E-10
Untreated +US	5.80E-01	1	2.90E-09	6.51E-08	6.98E-05	2.20E-07	4.48E-06	2.46E-10
DOX	2.90E-09	2.90E-09	1	3.88E-03	3.13E-04	2.76E-04	6.03E-04	9.19E-05
DOX+US	6.51E-08	6.51E-08	3.88E-03	1	1.93E-04	1.55E-04	2.89E-04	1.59E-04
CONTROL	6.98E-05	6.98E-05	3.13E-04	1.93E-04	1	2.22E-03	1.23E-02	7.37E-04
CONTROL +US	2.20E-07	2.20E-07	2.76E-04	1.55E-04	2.22E-03	1	4.12E-02	4.55E-03
ALB-DOX	4.48E-06	4.48E-06	6.03E-04	2.89E-04	1.23E-02	4.12E-02	1	3.18E-03
ALB-DOX+US	2.46E-10	2.46E-10	9.19E-05	1.59E-04	7.37E-04	4.55E-03	3.18E-03	1

However, the action of the control liposomes in the presence of US did not differ between both cell lines (p-value= 5.16×10^{-1}), signifying the effects of active targeting. Consequently, it is concluded that active-targeting combined with US exposure, yields the most promising results, and enhances receptor-mediated endocytosis in the receptor-overexpressing cell line. Finally, based on comparisons of the percent viability of free DOX treated cells and those treated with liposomes, it is observed in all cell lines that the cytotoxicity of DOX is reduced upon its encapsulation into the liposomal formulations.

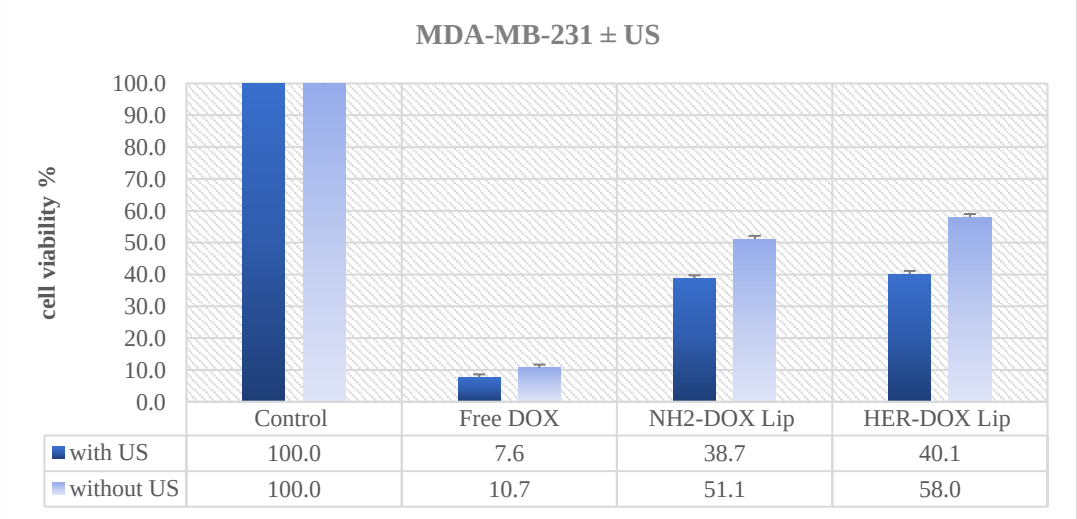

Figure 37: MDA-MB-231 cell viability % in response to different treatment groups. Data are representative of three independent experiments.

Table 8: Heat map summarizing p-values for the MDA-MB-231 cell line.

	Untreated	Untreated +US	DOX	DOX+US	CONTROL	CONTROL +US	HER-DOX	HER-DOX+US
Untreated	1	9.58E-01	7.64E-10	4.17E-10	2.01E-07	5.76E-08	2.68E-04	2.54E-10
Untreated +US	9.58E-01	1	7.64E-10	4.17E-10	2.01E-07	5.76E-08	2.68E-04	2.54E-10
DOX	7.64E-10	7.64E-10	1	1.55E-03	6.25E-07	2.03E-06	1.71E-04	1.03E-07
DOX+US	4.17E-10	4.17E-10	1.55E-03	1	4.33E-07	1.23E-06	1.33E-04	4.81E-08
CONTROL	2.01E-07	2.01E-07	6.25E-07	4.33E-07	1	1.60E-04	1.24E-01	8.44E-05
CONTROL +US	5.76E-08	5.76E-08	2.03E-06	1.23E-06	1.60E-04	1	5.48E-03	9.42E-02
HER-DOX	2.68E-04	2.68E-04	1.71E-04	1.33E-04	1.24E-01	5.48E-03	1	6.78E-03
HER-DOX+US	2.54E-10	2.54E-10	1.03E-07	4.81E-08	8.44E-05	9.42E-02	6.78E-03	1

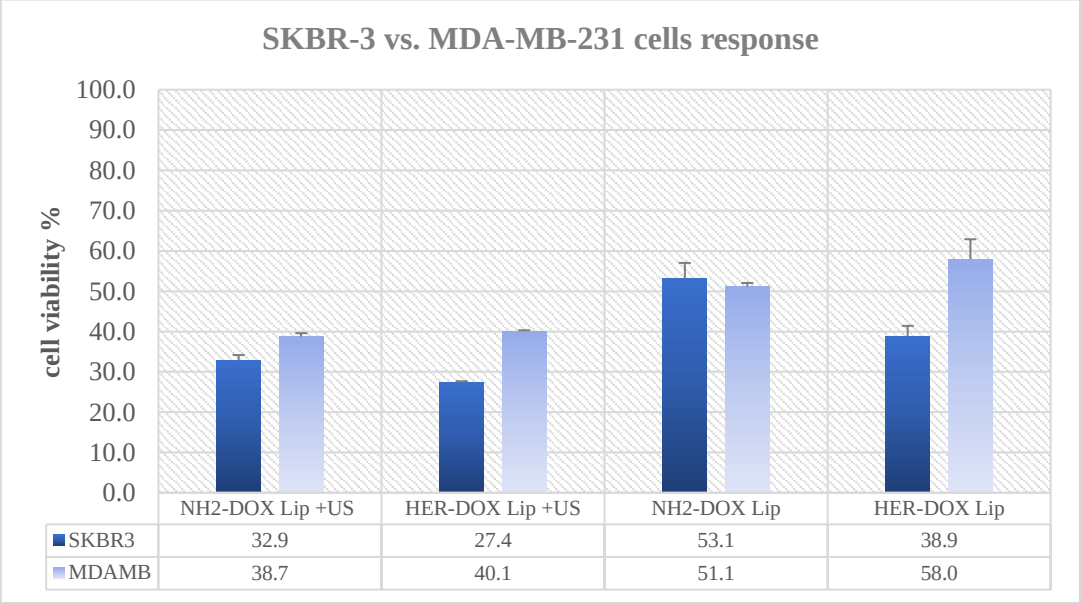

Figure 38: comparison of the cell viability % of the SKBR-3 vs. MDA-MB-231 cell lines.

A supporting study conducted by Alyane et al. [98] used flow cytometry and confocal microscopy imaging to compare the toxicity of free DOX and that of liposomes-entrapped in H9C2 cells. Figure 39 shows the confocal microscopy images of cells incubated with free DOX (A) and liposomes-entrapped (B) for 3 hours. The stronger fluorescence in the figure indicated a higher cellular accumulation of DOX. Therefore, the study concluded that the DOX toxicity was significantly reduced when encapsulated in liposomes, up to an incubation period of 20 hours, after which the encapsulated DOX became more toxic than the free one.

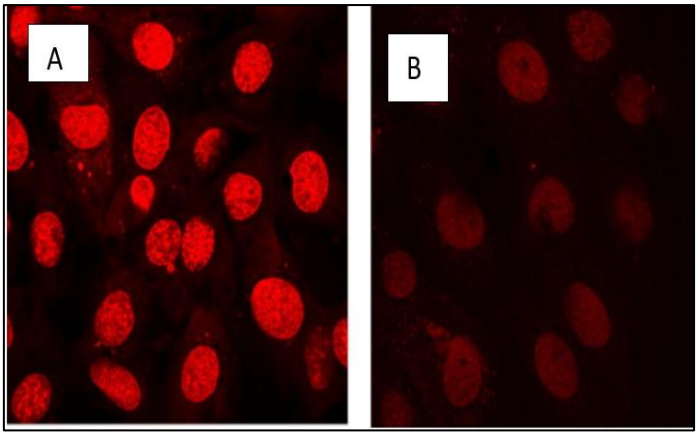

Figure 39: confocal microscopy images of H9C2 cells [98]

4.4. SPSS Analysis Results

Comparative statistical analyses were carried out on the quantitative data generated in this study. This section summarizes the results of the statistical analysis carried out using the SPSS software. To validate the choice of the test, Levene's test for equality of variances was carried out. The significance of the F-value was greater than 0.05 in all cases, confirming the assumption of equal variances.

Figures 40 through 51 in the appendix show the significant difference values (p-values) and Levene's test significance values computed using the software, comparing the treatment groups in the presence and absence of US, for each of the cell lines. The same p-value results can be extracted from the heat maps discussed above.

Upon evaluation of the t-test results:

- The 1st null hypothesis is safely rejected, because as seen from the previous discussion, US has a synergistic effect on the performance of all liposomal formulations, whether the conjugated or the unconjugated ones. Also, US has a significant effect on the performance of the free drug on the cells, confirming the effects of sonoporation in enhancing the cells' reception to the drug.
- The 2nd null hypothesis is also rejected because the effects of active targeting are profound when comparing the performance of the conjugated versus the unconjugated liposomes on the positive cell lines. Less cell viability percentages are observed in the positive cell line group of cells treated with the conjugated liposomes. The effect of active targeting is further enhanced in the presence of US, which again supports rejecting the 1st null hypothesis.

- The 3rd null hypothesis is accepted because it is anticipated and expected that conjugation will not significantly affect the negative cell line's cells, as they do not overexpress the receptors on their surface.

Also, it can be observed that all the Levene's test significance values are greater than 0.05 for all comparisons, which confirms the assumption of equal variances, confirming the appropriateness of the t-test choice.

Moreover, SPSS was used to compute the Chronbach's alpha value for the different sets of data, which is an indicator of the reliability and consistency of the measurements. The Chronbach's alpha values obtained are summarized in Table 9. The close to unity values indicate that the measurements of each data set are consistent and precise. A sensitivity and reliability test is an important indicator in biostatistics that eliminates chances of randomness and inconsistencies, especially when it comes to cancer treatment *in vitro* studies, which involve the use of live mutant cells.

Table 9: Chronbach's Alpha for each cell line's data set.

SKBR-3	MDA-MB-231
Reliability Statistics Cronbach's Alpha: .851 N of Items: 3	**Reliability Statistics** Cronbach's Alpha: .826 N of Items: 3
MCF-7	**HeLa**
Reliability Statistics Cronbach's Alpha: .789 N of Items: 3	**Reliability Statistics** Cronbach's Alpha: .851 N of Items: 3

Chapter 5. Conclusion

Intensive efforts in drug delivery aim to explore modalities that would combat the drawbacks of the currently available ones, which pose detriments for researchers and patients alike. One of the most well-established advances is state-of-the-art nanocarriers incorporated in smart drug delivery systems (SDDSs). SDDSs are nanoplatforms with important characteristics and bio-functions, that make them optimal for the remote delivery of drugs to targeted sites under controlled release conditions.

Also, the release mechanisms of such systems are controlled and can be tuned to be stimuli-responsive to endogenous or exogenous triggers, which is an added controlling advantage. Disadvantages associated with traditional chemotherapy such as nonselective systemic activity, poor drug solubility, hepatic biodegradation, dose-limiting toxicity, and the deterioration of the healthy cells can all be overcome using nanoparticles (NPs) as drug delivery vehicles.

In this thesis, synthesis, characterization and *in vitro* cell work of HSA-conjugated and HER-conjugated targeted liposomes with ultrasound (US) triggering were thoroughly considered. Size measurements of the control liposomes loaded with DOX, HSA-conjugated liposomes, and HER-conjugated liposomes revealed that the conjugated ones have larger radii compared to the control; yet, their size did not exceed the limits of the EPR requirement. Moreover, conjugation was confirmed, and the HSA-conjugated liposomes contained 5.5 more protein content, whereas the HER-conjugated liposomes contained 1.5 more protein content, compared to the control liposomes.

Finally, the *in vitro* assessment done on the different cell lines in the presence and absence of US exposure suggested that coupling US with active targeting elicits synergistic effects and enhanced drug uptake by the cells. Also, liposomal treatments, i.e., control and targeted, along with US exposure, showed more pronounced effects in both cell lines, as the observed cell viabilities were significantly less than in control non-sonicated cells.

In conclusion, this study supports and proves the synergistic effects of combining US as an external drug release modality with active targeting using a moiety. The applicability of the findings can form a baseline for future optimization efforts for the *in vitro* tests. To further extend this thesis in the future, it is recommended to

investigate the effects of different concentrations of the liposomal formulations on the cell lines, and to formulate clear dose-time, dose-US exposure and dose-cell line type relationships; which would be very useful when trying to translate the outcomes to potential *in vivo* experiments.

References

[1] "What Is Cancer? - National Cancer Institute." https://www.cancer.gov/about-cancer/understanding/what-is-cancer (accessed Apr. 25, 2020).

[2] R. L. Siegel, K. D. Miller, and A. Jemal, "Cancer statistics, 2020," *CA: A Cancer Journal for Clinicians*, vol. 70, no. 1, pp. 7–30, Jan. 2020.

[3] E. J. Benjamin *et al.*, "Heart Disease and Stroke Statistics-2019 Update: A Report From the American Heart Association," *Circulation*, vol. 139, no. 10, pp. e56–e528, Mar. 2019.

[4] J. C. Barrett, "Mechanisms of Multistep Carcinogenesis and Carcinogen Risk Assessment," 1993. Accessed: Apr. 25, 2020. [Online].

[5] R. K. Boutwell and A. Sivak, "The function and mechanism of promoters of carcinogenesis," *Critical Reviews in Toxicology*, vol. 2, no. 4, pp. 419–444, 1973.

[6] D. J. Hicklin and L. M. Ellis, "Role of the vascular endothelial growth factor pathway in tumor growth and angiogenesis," *Journal of Clinical Oncology*, vol. 23, no. 5. pp. 1011–1027, Apr. 2005.

[7] "Understanding Cancer: Metastasis, Stages of Cancer, and More." https://www.onhealth.com/content/1/cancer_types_treatments (accessed Apr. 30, 2020).

[8] "Immunotherapy for Cancer - National Cancer Institute." https://www.cancer.gov/about-cancer/treatment/types/immunotherapy (accessed Apr. 30, 2020).

[9] A. IMRAN *et al.*, "Role of Molecular Biology in Cancer Treatment: A Review Article," *Iranian Journal of Public Health*, vol. 46, no. 11, pp. 1475-1477, Mar. 2017, Accessed: Apr. 30, 2020. [Online].

[10] D. M. McDonald, "New Antibody to Stop Tumor Angiogenesis and Lymphatic Spread by Blocking Receptor Partnering," *Cancer Cell*, vol. 18, no. 6, pp. 541–543, Jan. 2010.

[11] Y. L. Li, H. Zhao, and X. B. Ren, "Relationship of VEGF/VEGFR with immune and cancer cells: staggering or forward?," *Cancer Biology and Medicine*, vol. 13, no. 2. Cancer Biology and Medicine, pp. 206–214, Mar. 2016.

[12] M. Arruebo *et al.*, "Assessment of the Evolution of Cancer Treatment Therapies," *Cancers*, vol. 3, no. 3, pp. 3279–3330, Mar. 2011.

[13] V. T. Devita and E. Chu, "A History of Cancer Chemotherapy," *Iranian Journal of Public Health*, vol. 41, no. 8, pp. 1512-1519, Apr. 2008.

[14] C. Carvalho *et al.*, "Doxorubicin: The Good, the Bad and the Ugly Effect," *Current Medicinal Chemistry*, vol. 16, no. 25, pp. 3267–3285, Jan. 2009.

[15] J. Kress *et al.*, "Quantitative imaging of light-triggered doxorubicin release," *Biomedical Optics Express*, vol. 6, no. 9, pp. 3640-3546, Sep. 2015.

[16] M. Volkova and R. Russell, "Anthracycline Cardiotoxicity: Prevalence, Pathogenesis and Treatment," *Current Cardiology Reviews*, vol. 7, no. 4, pp. 214–220, Mar. 2012.

[17] L. Zhao and B. Zhang, "Doxorubicin induces cardiotoxicity through upregulation of death receptors mediated apoptosis in cardiomyocytes," *Scientific Reports*, vol. 7, no. 1, pp. 1–11, Mar. 2017.

[18] D. Liu, F. Yang, F. Xiong, and N. Gu, "The smart drug delivery system and its clinical potential," *Theranostics*, vol. 6, no. 9, pp. 1306–1323, Jan. 2016.

[19] E. Pérez-Herrero and A. Fernández-Medarde, "Advanced targeted therapies in cancer: Drug nanocarriers, the future of chemotherapy," *European Journal of Pharmaceutics and Biopharmaceutics*, vol. 93, pp. 52–79, Jun. 2015.

[20] "Drug Delivery Group | American University of Sharjah." https://www.aus.edu/faculty/dr-rana-sabouni/drug-delivery-group (accessed Apr. 30, 2020).

[21] A. H. Faraji and P. Wipf, "Nanoparticles in cellular drug delivery," *Bioorganic and Medicinal Chemistry*, vol. 17, no. 8, pp. 2950–2962, Apr. 2009.

[22] S. al Basha, N. Salkho, S. Dalibalta, and G. A. Husseini, "Liposomes in Active, Passive and Acoustically-Triggered Drug Delivery," *Mini-Reviews in Medicinal Chemistry*, vol. 19, no. 12, pp. 961–969, Apr. 2019.

[23] M. R. Dreher, W. Liu, C. R. Michelich, M. W. Dewhirst, F. Yuan, and A. Chilkoti, "Tumor vascular permeability, accumulation, and penetration of macromolecular drug carriers," *Journal of the National Cancer Institute*, vol. 98, no. 5, pp. 335–344, Mar. 2006.

[24] D. R. Bielenberg and B. R. Zetter, "The Contribution of Angiogenesis to the Process of Metastasis," *Cancer Journal (United States)*, vol. 21, no. 4, pp. 267–273, Jul. 2015.

[25] P. Milla, F. Dosio, and L. Cattel, "PEGylation of Proteins and Liposomes: a Powerful and Flexible Strategy to Improve the Drug Delivery," *Current Drug Metabolism*, vol. 13, no. 1, pp. 105–119, Dec. 2011.

[26] F. Danhier, O. Feron, and V. Préat, "To exploit the tumor microenvironment: Passive and active tumor targeting of nanocarriers for anti-cancer drug delivery," *Journal of Controlled Release*, vol. 148, no. 2. pp. 135–146, Dec. 2010.

[27] P. Kumar, P. Huo, and B. Liu, "Formulation strategies for folate-targeted liposomes and their biomedical applications," *Pharmaceutics*, vol. 11, no. 8, pp. 381-382, Aug. 2019.

[28] K. Cho, X. Wang, S. Nie, Z. Chen, and D. M. Shin, "Therapeutic nanoparticles for drug delivery in cancer," *Clinical Cancer Research*, vol. 14, no. 5, pp. 1310–1316, Mar. 2008.

[29] K. Miyata, R. J. Christie, and K. Kataoka, "Polymeric micelles for nano-scale drug delivery," *Reactive and Functional Polymers*, vol. 71, no. 3, pp. 227–234, Mar. 2011.

[30] E. v. Batrakova, T. K. Bronich, J. A. Vetro, and A. v. Kabanov, “Polymer micelles as drug carriers,” in *Nanoparticulates as Drug Carriers*, Imperial College Press, 2006, pp. 57–93.

[31] S. E. Ahmed, A. M. Martins, and G. A. Husseini, “The use of ultrasound to release chemotherapeutic drugs from micelles and liposomes,” *Journal of Drug Targeting*, vol. 23, no. 1, pp. 16–42, Jan. 2015.

[32] A. A. Barba, S. Bochicchio, A. Dalmoro, and G. Lamberti, “Lipid delivery systems for nucleic-acid-based-drugs: From production to clinical applications,” *Pharmaceutics*, vol. 11, no. 8, Aug. 2019.

[33] N. Filipczak, J. Pan, S. S. K. Yalamarty, and V. P. Torchilin, “Recent advancements in liposome technology,” *Advanced Drug Delivery Reviews*, vol. 21, no. 11, pp. 12–14, Jun. 2020.

[34] S. Ota, S. Yoshizawa, and S. Takeuchi, “Microfluidic formation of monodisperse, cell-sized, and unilamellar vesicles,” *Angewandte Chemie - International Edition*, vol. 48, no. 35, pp. 6533–6537, Aug. 2009.

[35] A. Jahn, W. N. Vreeland, M. Gaitan, and L. E. Locascio, “Controlled Vesicle Self-Assembly in Microfluidic Channels with Hydrodynamic Focusing,” *Journal of the American Chemical Society*, vol. 126, no. 9, pp. 2674–2675, Mar. 2004.

[36] S. Pautot, B. J. Frisken, and D. A. Weitz, “Production of unilamellar vesicles using an inverted emulsion,” *Langmuir*, vol. 19, no. 7, pp. 2870–2879, Apr. 2003.

[37] E. Kastner, R. Kaur, D. Lowry, B. Moghaddam, A. Wilkinson, and Y. Perrie, “High-throughput manufacturing of size-tuned liposomes by a new microfluidics method using enhanced statistical tools for characterization,” *International Journal of Pharmaceutics*, vol. 477, no. 1–2, pp. 361–368, Dec. 2014.

[38] G. T. Noble, J. F. Stefanick, J. D. Ashley, T. Kiziltepe, and B. Bilgicer, “Ligand-targeted liposome design: Challenges and fundamental considerations,” *Trends in Biotechnology*, vol. 32, no. 1, pp. 32–45, Jan. 2014.

[39] N. S. Awad *et al.*, “Effect of Pegylation and Targeting Moieties on the Ultrasound-Mediated Drug Release from Liposomes,” *ACS Biomaterials Science and Engineering*, vol. 6, no. 1, pp. 48–57, Jan. 2020.

[40] Y. Matsumura *et al.*, “Phase I and pharmacokinetic study of MCC-465, a doxorubicin (DXR) encapsulated in PEG immunoliposome, in patients with metastatic stomach cancer,” *Annals of Oncology*, vol. 15, no. 3, pp. 517–525, Mar. 2004.

[41] X. Zhou *et al.*, “Lactosylated liposomes for targeted delivery of doxorubicin to hepatocellular carcinoma,” *International Journal of Nanomedicine*, vol. 7, pp. 5465–5474, Mar. 2012.

[42] W. Li *et al.*, “RGD-targeted paramagnetic liposomes for early detection of tumor: In vitro and in vivo studies,” *European Journal of Radiology*, vol. 80, no. 2, pp. 598–606, Nov. 2011.

[43] K. Laginha, D. Mumbengegwi, and T. Allen, “Liposomes targeted via two different antibodies: Assay, B-cell binding and cytotoxicity,” *Biochimica et Biophysica Acta - Biomembranes*, vol. 117, no. 1, pp. 25–32, Jun. 2005.

[44] R. J. Lee and P. S. Low, “Delivery of liposomes into cultured KB cells via folate receptor-mediated endocytosis,” *Journal of Biological Chemistry*, vol. 269, no. 5, pp. 3198–3204, Feb. 1994.

[45] A. Gabizon *et al.*, “Improved therapeutic activity of folate-targeted liposomal doxorubicin in folate receptor-expressing tumor models,” *Cancer Chemotherapy and Pharmacology*, vol. 66, no. 1, pp. 43–52, May 2010.

[46] R. N. Moman and M. Varacallo, *Physiology, Albumin*. StatPearls Publishing, 2019.

[47] H. Sun *et al.*, “HnRNPM and CD44s expression affects tumor aggressiveness and predicts poor prognosis in breast cancer with axillary lymph node metastases,” *Genes Chromosomes and Cancer*, vol. 56, no. 8, pp. 598–607, Aug. 2017.

[48] H. Satoh *et al.*, “Expression of hnRNP A2/B1 proteins in human cancer cell lines.,” *International journal of oncology*, vol. 16, no. 4, pp. 763–767, Mar. 2000.

[49] W. H. Yang, M. J. Ding, G. Z. Cui, M. Yang, and D. L. Dai, “Heterogeneous nuclear ribonucleoprotein M promotes the progression of breast cancer by regulating the axin/β-catenin signaling pathway,” *Biomedicine and Pharmacotherapy*, vol. 105, no. 11, pp. 848–855, Sep. 2018.

[50] S. M. Motevalli *et al.*, “Co-encapsulation of curcumin and doxorubicin in albumin nanoparticles blocks the adaptive treatment tolerance of cancer cells,” *Biophysics Reports*, vol. 5, no. 2, pp. 133-140, Mar. 2018.

[51] L. Dean, *Trastuzumab (Herceptin) Therapy and ERBB2 (HER2) Genotype*. National Center for Biotechnology Information (US), 2012.

[52] T. Vu and F. X. Claret, “Trastuzumab: Updated mechanisms of action and resistance in breast cancer,” *Frontiers in Oncology*, vol. 2, no. 6, pp. 12-16, Jun. 2012.

[53] J. L. Nordstrom *et al.*, “Anti-tumor activity and toxicokinetics analysis of MGAH22, an anti-HER2 monoclonal antibody with enhanced Fcγ receptor binding properties,” *Breast Cancer Research*, vol. 13, no. 6, Nov. 2011.

[54] L. Arnould *et al.*, “Trastuzumab-based treatment of HER2-positive breast cancer: An antibody-dependent cellular cytotoxicity mechanism?,” *British Journal of Cancer*, vol. 94, no. 2, pp. 259–267, Jan. 2006.

[55] D. M. Collins, N. O’donovan, P. M. Mcgowan, F. O’sullivan, M. J. Duffy, and J. Crown, “Trastuzumab induces antibody-dependent cell-mediated cytotoxicity (ADCC) in HER-2-non-amplified breast cancer cell lines,” *Annals of Oncology*, vol. 23, no. 7, pp. 1788–1795, Jul. 2012.

[56] W. Chen *et al.*, “Trastuzumab enhances the anti-tumor effects of the histone deacetylase inhibitor sodium butyrate on a HER2-overexpressing breast cancer

cell line," *International Journal of Molecular Medicine*, vol. 28, no. 6, pp. 985–991, Dec. 2011.

[57] D. Kirpotin *et al.*, "Sterically stabilized anti-HER2 immunoliposomes: Design and targeting to human breast cancer cells in vitro," *Biochemistry*, vol. 36, no. 1, pp. 66–75, Jan. 1997.

[58] J. W. Park *et al.*, "Tumor targeting using anti-her2 immunoliposomes," in *Journal of Controlled Release*, vol. 74, no. 1–3, pp. 95–113, Jul. 2001.

[59] K. M. Laginha, E. H. Moase, N. Yu, A. Huang, and T. M. Allen, "Bioavailability and therapeutic efficacy of HER2 scFv-targeted liposomal doxorubicin in a murine model of HER2-overexpressing breast cancer," *Journal of Drug Targeting*, vol. 16, no. 7, pp. 605–610, Aug. 2008.

[60] A. Bandekar, S. Karve, M. Y. Chang, Q. Mu, J. Rotolo, and S. Sofou, "Antitumor efficacy following the intracellular and interstitial release of liposomal doxorubicin," *Biomaterials*, vol. 33, no. 17, pp. 4345–4352, Jun. 2012.

[61] W. G. Pitt, G. Husseini, and B. J. Staples, "Ultrasonic drug delivery - A general review," *Expert Opinion on Drug Delivery*, vol. 1, no. 1, pp. 37–56, Nov. 2004.

[62] T. Boissenot, A. Bordat, E. Fattal, and N. Tsapis, "Ultrasound-triggered drug delivery for cancer treatment using drug delivery systems: From theoretical considerations to practical applications," *Journal of Controlled Release*, vol. 241, no. 129, pp. 144–163, Nov. 2016.

[63] P. Wang, Y. Li, X. Wang, L. Guo, X. Su, and Q. Liu, "Membrane damage effect of continuous wave ultrasound on K562 human leukemia cells," *Journal of Ultrasound in Medicine*, vol. 31, no. 12, pp. 1977–1986, Dec. 2012.

[64] H. Moussa, A. Martins, and G. Husseini, "Review on Triggered Liposomal Drug Delivery with a Focus on Ultrasound," *Current Cancer Drug Targets*, vol. 15, no. 4, pp. 282–313, Mar. 2015.

[65] A. Schroeder, J. Kost, and Y. Barenholz, "Ultrasound, liposomes, and drug delivery: principles for using ultrasound to control the release of drugs from liposomes," *Chemistry and Physics of Lipids*, vol. 162, no. 2. pp. 1–16, Nov. 2009.

[66] A. Schroeder, R. Honen, K. Turjeman, A. Gabizon, J. Kost, and Y. Barenholz, "Ultrasound triggered release of cisplatin from liposomes in murine tumors," *Journal of Controlled Release*, vol. 137, no. 1, pp. 63–68, Jul. 2009.

[67] M. B. C. de Matos *et al.*, "Ultrasound-Sensitive Liposomes for Triggered Macromolecular Drug Delivery: Formulation and In Vitro Characterization," *Frontiers in Pharmacology*, vol. 10, no. 12, pp. 1462-1463, Dec. 2019.

[68] G. A. Husseini, M. A. Diaz De La Rosa, E. S. Richardson, D. A. Christensen, and W. G. Pitt, "The role of cavitation in acoustically activated drug delivery," *Journal of Controlled Release*, vol. 107, no. 2, pp. 253–261, Oct. 2005.

[69] G. A. Husseini, R. I. El-Fayoumi, K. L. O'Neill, N. Y. Rapoport, and W. G. Pitt, "DNA damage induced by micellar-delivered doxorubicin and ultrasound: comet assay study.," *Cancer letters*, vol. 154, no. 2, pp. 211–214, Jun. 2000.

[70] G. A. Husseini and W. G. Pitt, “The use of ultrasound and micelles in cancer treatment,” *Journal of Nanoscience and Nanotechnology*, vol. 8, no. 5, pp. 2205–2215, May 2008.

[71] R. E. Apfel and C. K. Holland, “Gauging the likelihood of cavitation from short-pulse, low-duty cycle diagnostic ultrasound,” *Ultrasound in Medicine and Biology*, vol. 17, no. 2, pp. 179–185, Jan. 1991.

[72] A. Schroeder, J. Kost, and Y. Barenholz, “Ultrasound, liposomes, and drug delivery: principles for using ultrasound to control the release of drugs from liposomes,” *Chemistry and Physics of Lipids*, vol. 162, no. 1, pp. 1–16, Nov. 2009.

[73] K. Tachibana, T. Uchida, K. Ogawa, N. Yamashita, and K. Tamura, “Induction of cell-membrane porosity by ultrasound,” *Lancet*, vol. 353, no. 62, pp. 1402-1409, Apr. 1999.

[74] T. Mosmann, “Rapid Colorimetric Assay for Cellular Growth and Survival: Application to Proliferation and Cytotoxicity Assays,” 1983. Accessed: Apr. 30, 2020. [Online].

[75] “Protocol Guide: MTT Assay for Cell Viability and Proliferation | Sigma-Aldrich.”https://www.sigmaaldrich.com/technical-documents/protocols/biology/roche/cell-proliferation-kit-i-mtt.html (accessed Apr. 30, 2020).

[76] W. G. Pitt *et al.*, “Preliminary results of combining low frequency low intensity ultrasound and liposomal drug delivery to treat tumors in rats,” in *Journal of Nanoscience and Nanotechnology*, vol. 11, no. 3, pp. 1866–1870, Mar. 2011.

[77] K. Saito, K. Miyake, P. L. McNeil, K. Kato, K. Yago, and N. Sugai, “Plasma membrane disruption underlies injury of the corneal endothelium by ultrasound,” *Experimental Eye Research*, vol. 68, no. 4, pp. 431–437, Apr. 1999.

[78] N. Y. Rapoport, J. N. Herron, W. G. Pitt, and L. Pitina, “Micellar delivery of doxorubicin and its paramagnetic analog, ruboxyl, to HL-60 cells: Effect of micelle structure and ultrasound on the intracellular drug uptake,” *Journal of Controlled Release*, vol. 58, no. 2, pp. 153–162, Mar. 1999.

[79] N. Munshi, N. Rapoport, and W. G. Pitt, “Ultrasonic activated drug delivery from Pluronic P-105 micelles,” *Cancer Letters*, vol. 118, no. 1, pp. 13–19, Sep. 1997.

[80] E. L. Yuh *et al.*, “Delivery of systemic chemotherapeutic agent to tumors by using focused ultrasound: Study in a murine model,” *Radiology*, vol. 234, no. 2, pp. 431–437, Feb. 2005.

[81] E. Thomas *et al.*, “Ultrasound-mediated cavitation enhances the delivery of an EGFR-targeting liposomal formulation designed for chemo-radionuclide therapy,” *Theranostics*, vol. 9, no. 19, pp. 5595–5609, Jun. 2019.

[82] N. M. Salkho *et al.*, “Ultrasonically controlled estrone-modified liposomes for estrogen-positive breast cancer therapy,” *Artificial Cells, Nanomedicine and Biotechnology*, vol. 46, no. 25, pp. 462–472, Nov. 2018.

[83] N. S. Awad, V. Paul, M. H. Al-Sayah, and G. A. Husseini, “Ultrasonically controlled albumin-conjugated liposomes for breast cancer therapy,” *Artificial Cells, Nanomedicine, and Biotechnology*, vol. 47, no. 1, pp. 705–714, Dec. 2019.

[84] Y. Okamoto, K. Taguchi, S. Imoto, V. T. Giam Chuang, K. Yamasaki, and M. Otagiri, “Cell uptake and anti-tumor effect of liposomes containing encapsulated paclitaxel-bound albumin against breast cancer cells in 2D and 3D cultured models,” *Journal of Drug Delivery Science and Technology*, vol. 55, no. 21, pp. 99-101, Feb. 2020.

[85] H. Xing *et al.*, “Selective delivery of an anticancer drug with aptamer-functionalized liposomes to breast cancer cells in vitro and in vivo,” *Journal of Materials Chemistry B*, vol. 1, no. 39, pp. 5288–5297, Oct. 2013.

[86] H. Bardania *et al.*, “RGD-modified nano-liposomes encapsulated eptifibatide with proper hemocompatibility and cytotoxicity effect,” *Iranian Journal of Biotechnology*, vol. 17, no. 2, pp. 8–13, Mar. 2019.

[87] H. Zhang, “Thin-film hydration followed by extrusion method for liposome preparation,” in *Methods in Molecular Biology*, vol. 1522, no. 98, pp. 17–22, Mar. 2017.

[88] A. Fritze, F. Hens, A. Kimpfler, R. Schubert, and R. Peschka-Süss, “Remote loading of doxorubicin into liposomes driven by a transmembrane phosphate gradient,” *Biochimica et Biophysica Acta - Biomembranes*, vol. 1758, no. 10, pp. 1633–1640, Oct. 2006.

[89] “LUNA-II Cell Counter - Fast, Accurate & Affordable Cell Counting.” https://www.westburg.eu/products/cell-biology/cell-counting/automated-cell-counter-luna-ii (accessed Sep. 29, 2020).

[90] S. Peretz Damari *et al.*, “Practical aspects in size and morphology characterization of drug-loaded nano-liposomes,” *International Journal of Pharmaceutics*, vol. 547, no. 12, pp. 648–655, Aug. 2018.

[91] M. Kaszuba, D. McKnight, M. T. Connah, F. K. McNeil-Watson, and U. Nobbmann, “Measuring sub nanometre sizes using dynamic light scattering,” *Journal of Nanoparticle Research*, vol. 10, no. 5, pp. 823–829, May 2008.

[92] J. C. M. Stewart, “Colorimetric determination of phospholipids with ammonium ferrothiocyanate,” *Analytical Biochemistry*, vol. 104, no. 1, pp. 10–14, May 1980.

[93] M. T. Hussain, N. Forbes, and Y. Perrie, “Comparative analysis of protein quantification methods for the rapid determination of protein loading in liposomal formulations,” *Pharmaceutics*, vol. 11, no. 1, Jan. 2019.

[94] M. Tavakol and R. Dennick, “Making sense of Cronbach’s alpha,” *International journal of medical education*, vol. 2, no. 6, pp. 53–55, Jun. 27, 2011.

[95] H. Hsu and P. A. Lachenbruch, “Paired t Test,” in *Encyclopedia of Biostatistics*, Chichester, UK: John Wiley & Sons, Ltd, 2005.

[96] T. K. Kim, “T test as a parametric statistic,” *Korean Journal of Anesthesiology*, vol. 68, no. 6, pp. 540–546, Dec. 2015.

[97] Y. Jiang, S. Wong, F. Chen, T. Chang, H. Lu, and M. H. Stenzel, “Influencing Selectivity to Cancer Cells with Mixed Nanoparticles Prepared from Albumin-Polymer Conjugates and Block Copolymers,” *Bioconjugate Chemistry*, vol. 28, no. 4, pp. 979–985, Apr. 2017.

[98] M. Alyane, G. Barratt, and M. Lahouel, “Remote loading of doxorubicin into liposomes by transmembrane pH gradient to reduce toxicity toward H9c2 cells,” *Saudi Pharmaceutical Journal*, vol. 24, no. 2, pp. 165–175, Mar. 2016.

Appendix: SPSS Results

1. Independent Samples Test and Levene's Test Results for SKBR-3 Cell Line

Independent Samples Test

		Levene's Test for Equality of Variances				
		F	Sig.	t	df	Sig. (2-tailed)
DOX	Equal variances assumed	2.980	.159	5.934	4	.004
	Equal variances not assumed			5.934	2.699	.013
NH2	Equal variances assumed	3.085	.154	6.955	4	.002
	Equal variances not assumed			6.955	2.450	.011
HER	Equal variances assumed	12.746	.450	6.260	4	.003
	Equal variances not assumed			6.260	2.042	.023

Figure 40: t-test Significance and Levene's test significance for comparison between free DOX. Control liposomes and HER-DOX liposomes treatments with and without US on SKBR-3 cells

Independent Samples Test

		Levene's Test for Equality of Variances				
		F	Sig.	t	df	Sig. (2-tailed)
NH2vsHERwithUS	Equal variances assumed	3.991	.116	5.675	4	.005
	Equal variances not assumed			5.675	2.158	.025

Figure 41: t-test Significance and Levene's test significance for comparison between Control liposomes and HER-DOX liposomes treatments with exposure to US on SKBR-3 cells

Independent Samples Test

		Levene's Test for Equality of Variances				
		F	Sig.	t	df	Sig. (2-tailed)
NH2vsHERwithoutUS	Equal variances assumed	.590	.485	4.312	4	.013
	Equal variances not assumed			4.312	3.455	.017

Figure 42: t-test Significance and Levene's test significance for comparison between Control liposomes and HER-DOX liposomes treatments without exposure to US on SKBR-3 cells

2. Independent Samples Test and Levene's Test Results for MDA-MB-231 Cell Line

Independent Samples Test

		Levene's Test for Equality of Variances				
		F	Sig.	t	df	Sig. (2-tailed)
DOX	Equal variances assumed	.093	.776	7.562	4	.002
	Equal variances not assumed			7.562	3.965	.002
NH2	Equal variances assumed	.033	.864	13.731	4	.000
	Equal variances not assumed			13.731	3.966	.000
HER	Equal variances assumed	5.326	.082	5.164	4	.007
	Equal variances not assumed			5.164	2.008	.035

Figure 43: t-test Significance and Levene's test significance for comparison between free DOX. Control liposomes and HER-DOX liposomes treatments with and without US on MDA-MB-231 cells

Independent Samples Test

		Levene's Test for Equality of Variances				
		F	Sig.	t	df	Sig. (2-tailed)
NH2vsHERwithUS	Equal variances assumed	2.209	.211	-2.185	4	.094
	Equal variances not assumed			-2.185	2.253	.146

Figure 44: t-test Significance and Levene's test significance for comparison between Control liposomes and HER-DOX liposomes treatments with exposure to US on MDA-MB-231 cells

Independent Samples Test

		Levene's Test for Equality of Variances				
		F	Sig.	t	df	Sig. (2-tailed)
NH2vsHERwithoutUS	Equal variances assumed	3.709	.126	-1.951	4	.123
	Equal variances not assumed			-1.951	2.148	.182

Figure 45: t-test Significance and Levene's test significance for comparison between CONTROL liposomes and HER-DOX liposomes treatments without exposure to US on MDA-MB-231 cells

3. Independent Samples Test and Levene's Test Results for MCF-7 Cell Line

Independent Samples Test

		Levene's Test for Equality of Variances				
		F	Sig.	t	df	Sig. (2-tailed)
DOX	Equal variances assumed	1.906	.240	13.582	4	.000
	Equal variances not assumed			13.582	2.453	.002
NH2	Equal variances assumed	3.109	.153	30.952	4	.000
	Equal variances not assumed			30.952	2.508	.000
ALB	Equal variances assumed	11.134	.450	16.593	4	.000
	Equal variances not assumed			16.593	2.097	.003

Figure 46: t-test Significance and Levene's test significance for comparison between free DOX. Control liposomes and ALB-DOX liposomes treatments with and without US on MCF-7 cells

Independent Samples Test

		Levene's Test for Equality of Variances				
		F	Sig.	t	df	Sig. (2-tailed)
NH2vsALBwithoutUS	Equal variances assumed	3.695	.127	3.607	4	.023
	Equal variances not assumed			3.607	2.821	.040

Figure 47: t-test Significance and Levene's test significance for comparison between Control liposomes and HER-DOX liposomes treatments with exposure to US on MCF-7 cells

Independent Samples Test

		Levene's Test for Equality of Variances				
		F	Sig.	t	df	Sig. (2-tailed)
NH2vsALBwithUS	Equal variances assumed	.192	.684	44.101	4	.000
	Equal variances not assumed			44.101	3.861	.000

Figure 48: t-test Significance and Levene's test significance for comparison between d liposomes and HER-DOX liposomes treatments without exposure to US on MCF-7 cells

4. Independent Samples Test and Levene's Test Results for Hela Cell Line

Independent Samples Test

		Levene's Test for Equality of Variances				
		F	Sig.	t	df	Sig. (2-tailed)
DOX	Equal variances assumed	.571	.492	20.889	4	.000
	Equal variances not assumed			20.889	3.723	.000
NH2	Equal variances assumed	12.738	.834	12.282	4	.000
	Equal variances not assumed			12.282	2.044	.006
ALB	Equal variances assumed	2.866	.166	66.414	4	.000
	Equal variances not assumed			66.414	2.666	.000

Figure 49: t-test Significance and Levene's test significance for comparison between free DOX. Control liposomes and ALB-DOX liposomes treatments with and without US on HeLa cells

Independent Samples Test

		Levene's Test for Equality of Variances				
		F	Sig.	t	df	Sig. (2-tailed)
NH2vsALBwithUS	Equal variances assumed	11.339	.028	-1.391	4	.237
	Equal variances not assumed			-1.391	2.087	.294

Figure 50: t-test Significance and Levene's test significance for comparison between Control liposomes and HER-DOX liposomes treatments with exposure to US on HeLa cells

Independent Samples Test

		Levene's Test for Equality of Variances				
		F	Sig.	t	df	Sig. (2-tailed)
NH2vsALBwithoutUS	Equal variances assumed	.518	.512	2.626	4	.058
	Equal variances not assumed			2.626	3.221	.073

Figure 51: t-test Significance and Levene's test significance for comparison between CONTROL liposomes and HER-DOX liposomes treatments without exposure to US on HeLa cells

Vita

Waad Hussein Abuwatfa was born in 1997, in Al Ain city, in the United Arab Emirates. She was educated in private schools and graduated high school from the Gulf International Private Academy (GIPA) as class valedictorian in 2014. She received her B.Sc. degree in Chemical Engineering and graduated cum laude from the American University of Sharjah (AUS) in 2018. In 2019, she rejoined the Chemical Engineering master's program at the American university of Sharjah. She was awarded a graduate assistantship which provided her with an opportunity to develop her research and teaching skills and to gain academia experience. Her current research focuses on developing and assessing the performance of nanoparticles-based smart drug delivery systems for the treatment of breast cancer.